CFD simulation of indoor-outdoor wind-driven ventilation and traffic pollutant dispersion at a T-shaped street intersection (ISHVAC 2023)

Chen, Meng-Ying, Sun, Jie, Zhong, H., Liu, Ya-Nan, Dong, Wei, Cai, Yang, Zhao, Fu-Yun, Qian, Fu-Ping and Jimenez-Bescos, Carlos

This is an accepted manuscript of an article published by Taylor & Francis in the International Journal of Ventilation.

The final definitive version is available online:

https://doi.org/10.1080/14733315.2024.2426402

Title

CFD Simulation of Indoor-outdoor Wind-driven Ventilation and Traffic Pollutant Dispersion at a T-shaped Street Intersection (ISHVAC 2023)

Meng-Ying Chen[1#], Jie Sun[1#], Huai-Yu Zhong[1*], Ya-Nan Liu[2], Wei Dong[3], Yang Cai[4], Fu-Yun Zhao[5], Fu-Ping Qian[1], Carlos Jimenez-Bescos[6]

(1) School of Energy and Environment, ***Anhui University of Technology***, Ma'anshan, Anhui Province, 243002, China
(2) School of Architecture and Urban Planning, Chongqing Jiaotong University, Chongqing, 400074, China
(3) School of Civil Engineering and Architecture, ***Anhui University of Technology***, Ma'anshan, Anhui Province, 243032, China
(4) Energy and Electricity Research Center, ***Jinan University***, Zhuhai, Guangdong Province, China
(5) School of Power and Mechanical Engineering, ***Wuhan University***, Wuhan, Hubei Province, 430072, China
(6) ***University of Westminster***, London, UK

[#] These two authors contributed equally and should be regarded as co-first authors.

* Author to whom all correspondence should be addressed.
Address: School of Energy and Environment, Anhui University of Technology, Ma'anshan, Anhui Province, 243002, China.
Emails: hyzhong@ahut.edu.cn, huaiyzhong@163.com (**Prof. Huai-Yu Zhong**)

Abstract and keywords

Abstract

Traffic exhaust is considered as a predominant pollutant source for buildings along streets. However, there are few studies on ventilation and pollution dispersion inside buildings and along streets in a T-shaped intersection. This study investigates the ventilation performance and pollutant dispersion inside and outside multi-unit buildings at T-shaped intersection at different wind directions. Different wind-driven ventilation modes have been compared, i.e. SS2 (single-sided ventilation with 2 openings) and CV (cross ventilation). Unsteady Reynolds-averaged Navier-Stokes (URANS) method with SST k-ω turbulent model is adopted to conduct the CFD simulations. The results show that multi-unit buildings have the potential to enhance SS2 ventilation performance. Generally, at T-shaped street intersections, the overall impact on ventilation performance for multi-unit SS2 buildings is positive under various wind directions. The diffusion of outdoor pollutants into indoor environments is more closely related to wind direction for SS2 than CV. Additionally, CV can improve both the ventilation performance and pollutant removal capabilities of multi-unit building. However, at certain wind direction (θ=135°), a significant increase in indoor pollutant concentrations is observed in CV, nearly tenfold higher than that in SS2 cases. The findings could contribute to the understanding of ventilation in multi-unit buildings at T-shaped street intersections.

Keywords

Wind-driven ventilation, T-shaped street intersection, Ventilation rate, Pollutant dispersion

Highlights

- Indoor-outdoor ventilation and pollution dispersion are studied.
- Ventilation performance of SS2 and CV are compared in a T-shaped intersection.
- Multi-unit building has better SS2 ventilation performance.
- Diffusion of pollutants is more closely related to wind direction for SS2 than CV.

Main text

1. Introduction

1.1 Importance of researching natural ventilation

Modern people are reported to live and work indoors for about 80 % of the day [1]. The maintenance of indoor air freshness and thermal comfort is considered extremely critical, resulting in significant energy usage by HVAC (Heating, Ventilation and Air Conditioning) systems [2]. It was reported that buildings account for approximately 40% of the total energy usage, with more than half of this energy consumption attributed to HVAC systems [3]. Natural ventilation (NV) is increasingly favored in sustainable urban building, a trend significantly fueled by the low-carbon concept [4].

NV might be seen as the fundamental process of opening windows to promote the building's ventilation through natural air movement. Actually, NV is anything but simple; delving into it requires pondering upon certain critical issues: (1) Which is susceptible to natural forces, in combination with environmental elements; (2) How to promote NV, considering the architectural elements; (3) Can NV still be utilized effectively when outdoor air is contaminated; etc. To conclude, the study of NV is acknowledged to be considerably more challenging than that of Mechanical Ventilation (MV) due to the variability of natural forces [5].

NV is commonly categorized into four distinct airflow patterns, which are determined by the positioning of openings. These ventilation mode classifications encompass four principal types: Single-Sided Ventilation (SSV), Corner Ventilation (CRV), Displacement Ventilation (DV), and Cross Ventilation (CV) [5]. However, despite its lower efficiency in terms of ventilation performance, SSV is more prevalently implemented in urban buildings, primarily due to the high density and closely packed design of both residential and commercial structures. Consequently, ventilation strategies such as CV, CRV, or SV are frequently constrained within the urban built environment. [6].

1.2 Studies on SSV

SSV is typically categorized based on the number of openings on the same façade, that is, SS1 (1 opening) and SSn (multiple (n) openings). The ventilation rate in SS1 is typically minimal. Researching have shown that SSn provides a higher ventilation rate than SS1, even though both have the same total opening area [7]. SS2 has been the most extensively studied configuration among the SSn series, as it effectively represents the airflow dynamics of the other SSn designs. [5-6].

The research finds that, for single-unit building, the ventilation rate of SS2 shows a high sensitivity to variations in the angle of the incoming wind [6, 8]. In windward ventilation, stable airflow and low turbulence result in the positive wind pressure dominating the SS2 ventilation rate (**Fig. 1(a)**). Shear ventilation triggers highly turbulent, unsteady flows, making shear layer fluctuations the main contributor to SS2 ventilation (**Fig. 1(b)**). Leeward ventilation involves a large recirculation vortex with negative pressure, driving the SS2 ventilation rate, with turbulence intensity between windward and shear conditions (**Fig. 1(c)**).

Moreover, the natural ventilation driving force is jointly acted upon by wind pressure and buoyancy. The wind pressure and buoyancy force can either enhance or inhibit each other, depending predominantly on the wind direction and the indoor-outdoor temperature difference [11]. Therefore, this paper focused on scenarios where the prevailing wind velocity is sufficiently high, thereby rendering the effects of buoyancy-driven ventilation negligible [12].

The environmental and architectural elements are the two types of elements mainly considered in studies about SS2. Previous research has focused on various architectural elements based on single-unit building, including the number/area of openings, their location, geometric shape, and surrounding structures. As the research advances, numerous studies have investigated the various impacts of multi-zonal effects on building ventilation performance [13-16]. Ai et al. [14] found CFD to be especially apt for forecasting ventilation rates in multi-unit buildings. Meanwhile, Ai et al. [15] also found that the indoor airflow organization is influenced by the relative positions within the building. Pan et al. [16], through field measurements, devised a predictive model capable of precisely estimating ventilation rates while elucidating the interaction between thermal buoyancy and wind pressure.

However, for multi-unit buildings, the existing studies have predominantly focused on scenarios involving single-opening, single-sided ventilation. They have not extensively investigated the case of single-sided ventilation with dual or multiple apertures.

1.3 Studies on pollution transmission in streets

Air quality and ventilation rate are the two major evaluation indicators for the natural ventilation performance of SS2. In urban settings, air pollutants originating from indoors can spread to other units via airborne pathways. However, the majority of studies in this area have predominantly centered on evaluating high-rise buildings [17]. Few study can be found in literature on indoor-outdoor dispersion of traffic pollutant at a T-shaped street intersection.

Generally, studies on traffic pollution dispersion at street intersection are limited to outdoor environment [18-23]. K. Ahmad et al. [18] conducted both wind tunnel experiment and CFD simulation to investigate the ventilation situations in various intersection designs. According to Dou et al.'s [19] research, the accumulation situation of pollutants in the downstream of traffic roads can be greatly affected by wind velocity. Guo et al. [20] studied street ventilation in with different intersection patterns. Soulhac et al. [21] conducted CFD simulations into airflow and pollutant transport mechanisms at a street intersection. Tan et al. [22] examined carbon dioxide diffusion in streets, considering wind direction and the source of leakage as contributing factors. Their results indicated that pollutant concentrations can be significantly influenced by changes in wind directions. Shen et al. [23] analyzed six real-world scenarios to explore the impact of street morphology (e.g., street width, lateral openings, and intersections) on street ventilation. The study unveiled the influence of lateral openings and intersections on street-level ventilation.

With the continuous advancement of computational technology, an increasing number of researchers are adopting a combined indoor-outdoor analytical approach to more comprehensively evaluate indoor ventilation volumes [24-26]. Ghorui et al. [24] investigated the optimal positioning of patients in rooms by altering the inlet and outlet configurations under the assumption of constant outdoor wind direction, finding that ventilation openings directly above patients were most effective. Tong et al. [25] assessed the indoor ventilation efficiency of centrally located tall buildings within building clusters. The ratio of street-facing to opposite-facing sides affects the flow of wind around tall buildings. Cure et al. [26] conducted modeling of real teaching buildings, analyzing classroom ventilation scenarios, and suggesting that cross-ventilation with chimney vents and inlet openings is beneficial for improving indoor conditions. However, existing studies fall short in providing a detailed exploration of the dispersion and distribution characteristics of pollutants indoors and outdoors on streets under SS2 conditions. Moreover, the influence of T-shaped street intersections on the ventilation performance of surrounding buildings and the dispersion of pollutants remains unclear.

1.4 Objective of this study

This research focuses on a comprehensive analysis of ventilation efficiency and pollutant dispersion characteristics under the SS2 mode. Moreover, prior research findings indicate a striking discrepancy in ventilation efficiency between cross ventilation (CV) and SS2. In multi-unit buildings, the difference in ventilation performance between SS2 and CV is unclear. To bridge the aforementioned gap, this study conducts CFD simulations to study the effect of wind direction conditions in T-shaped street intersection, considering the effect of SS2 and CV modes on ventilation performance and pollutant dispersion of multi-unit buildings. Notably, this paper considers T-shaped street intersections as a key factor in studying the impact of main streets and their adjacent side streets on the ventilation performance of rooms in surrounding buildings. The traffic volume and the resulting pollutant strength on the side street can be considered negligible compared with those on the main road.

2. Methodology of CFD simulations

2.1 Geometrical models

Fig. 2 depicts the single-unit model employed in this study, which is the basic unit of multi-unit building. The miniature model of this three-story building is a 1/30 reduce in proportion with dimensions of L × W × H = (30 × 30 × 30) cm^3. The height is consistent across each floor (= 10 cm). Considering the effects of ground-level viscous resistance and rooftop vortex shedding respectively on the ground floor and the top floor, the 2^{nd} floor, being an intermediate floor, is a more representative choice. In the author's previous work, the second floor was also the primary focus studied in the wind tunnel experiments and CFD simulations. Therefore, only the natural ventilation through the 2^{nd} floor has been investigated. **Fig. 2(a)** reveals the SS2 model in this research, the 2 openings are located on the same wall of the building and are symmetrical around the centerline of the single-unit building model, with the same dimensions ($L_W \times L_W$ = 5 cm × 5 cm). The distance separating two openings is (distance between the center of the two openings) S = 15 cm, resulting in a dimensionless spacing $s' = S/W = 0.50$. The structural building model employed herein mirrors the model we investigated during prior boundary-layer wind tunnel studies [31]. In addition, this study also considers the CV mode, as shown in **Fig. 2(b)**.

There are totally four types of case are studied in this paper, and all openings are the same in area and shape. The single-unit models illustrated in **Fig. 2** are assembled sequentially, so as to obtain the corresponding four case (Case A–D) shown in **Fig. 3**, where the areas of pollutant emission are emphasized in purple. Traffic emissions were modeled using sulfur hexafluoride (SF6) as a tracer gas, released from street-level sources, following the method detailed by Meroney et al. [27]. It should be noted that, the room name is denoted by [Room-number], e.g. [R-A], in which “R” is abbreviated. Furthermore, all the buildings have a side ratio of 1:10. Except for the specific instances of A and B, all the case consist of street canyons with an aspect ratio of 1.

In the study, each case is specifically labeled as follows: "Case i-φ", where i is the model types from A to D in **Fig. 3**. For instance, Case A-0 indicates Case A for wind direction (φ) of 0°. In particular, the north wind direction is taken to be 0°, and a 45° interval is adopted to consider the effect of changing wind direction.

2.2 Computational domain

The computational domain is established following to Ref. [28] (see **Fig. 4**). Its size is length × width × height = 63H × 45H × 3H, where H is represented the height of the building, Dy is the represented width of the building, Dx is represented the length of the building. The origin of the coordinate system is designated as the center of the street canyon's base. The buildings are set 5Dx away from the upstream boundary and 15Dx from the downstream boundary. The buildings are positioned with a distance of 7Dy from both side boundaries, and the top boundary is set at a height of 3H, giving rise to a blockage ratio of around 2.3%, which does not exceed the threshold value (3%) recommended in AIJ guidelines [29].

2.3 Solver settings & boundary conditions

This paper employs URANS method to conduct CFD simulations. Building upon the configurations of CFD solvers utilized in previous studies, the SST k-ω turbulence model exhibits superior accuracy compared to the k-ε model in predicting shear layers in the vicinity of walls [30], and hence it is widely employed in CFD simulations of natural ventilation and street canyon scenarios. **Table 1** presents the setting of the solver configurations and boundary condition parameters. The CFD simulation protocol encompassed both Steady SRANS and URANS methodologies. An initial stable flow field was attained through 2000 SRANS iterations preceding the URANS computations. A consistent time step of $\Delta t = 0.001$ seconds was maintained, aligned with the 1000 Hz measurement frequency reported in the Wind Tunnel Experiment (WTE) [31]. By comparing time-averaged velocity magnitudes at the opening center using time steps of $\Delta t = 0.005$ s and 0.0005 s, variation less than 1.00% confirmed the solution's insensitivity to time step variations. The Courant number hovered around 1 for the majority of cells in proximity to the building model, ensuring a balanced treatment of time and space with the adopted implicit solver, as required for stability [29]. Further, mean velocity magnitude deviations at the opening center, sampled over intervals of 50000, 60000, and 70000-time steps, remained below 1.00%, justifying the selection of the final 60000- time steps from the complete 100000-time step simulation for capturing fully developed flow fields.

The boundary conditions adopted are coincident with those employed in the author's previous WTE study [31]. The mean profile of stream-wise wind velocity $U(z)$ is expressed by the power law:

$$\frac{U(z)}{U_H} = (\frac{z}{H})^{\alpha} \tag{1}$$

Where U_H (= 6 m/s) is the wind velocity at the building's roof height (H), z is the vertical height, and the exponent for the power-law, α, is taken as 0.19.

In adherence to the guidelines stipulated by AIJ [40], the formulations for turbulent kinetic energy $k(z)$, the rate of turbulent energy dissipation $\varepsilon(z)$, and the specific dissipation rate $\omega(z)$ are delineated as follows:

$$k(z) = \big(I(z)U(z)\big)^2 \tag{2}$$

$$\varepsilon(z) = C_\mu^{\frac{1}{2}} k(z) \frac{dU(z)}{dz} \tag{3}$$

$$\omega(z) = \frac{\varepsilon(z)}{k(z)C_\mu} \tag{4}$$

where $C\mu$ (= 0.09) is a constant.

2.4 Gaseous pollutant modelling

According to the CODASC database [34], SF_6 (sulfur hexafluoride) is chosen as the contaminant species. In the case of the T-shaped street intersection (refer to **Fig. 3(b)**), the gaseous pollutant SF_6 is released evenly from two surface sources on the ground, each measuring 3000 cm in length and 6 cm in width, and they are equally spaced. The total emission rate of the SF_6 pollutant is Q (10 g/s). The zero normal flux condition at wall surfaces and zero normal gradient condition at domain outlet and domain roof are used. At domain inlet, the concentration is null.

The turbulent Schmidt number (Sc_t) is defined as the ratio of turbulent momentum diffusivity (eddy viscosity) (V_t) and turbulent mass diffusivity (D_t) ($Sc_t = V_t/D_t$). It is known that Sc_t may vary depending on different turbulent flow structures and dispersion problems, but in CFD simulations it is usually treated as a constant ranging from 0.2 to 1.3 [38]. $Sc_t = 0.5$ is finally adopted in this study, which is consistent with that in the WTE [34].

2.5 Grid independence analysis

Hybrid meshes are adopted in all grids of the present study, and the orthogonal mass of the grid is greater than 0.36. The architectural model is nested in a rectangular block 12 times larger than itself. This arrangement makes it easier to generate a sufficiently fine grid near the surface of the building, while leaving the grid in a rougher state in areas away from the building. Grid independence analysis is conducted based on the Case C-0. Three mesh schemes (coarse, medium and fine) are generated. The number of grids for each scheme is: 2.79 million, 3.56 million and 6.27 million respectively. **Fig. 5** illustrates the visual representation of the grid configuration designed for the fundamental scenario. The total number of meshes is different due to the difference of dimensionless near wall distance y^+, stretch ratio and boundary layer number. The grid details are presented in **Table 2**.

To assess the accuracy of the simulation results for differing mesh sizes, the Grid Convergence Index (GCI) method developed by Roache is utilized [32]. Six Vertical profiles were selected within the street and indoor areas. Wind velocities(U) and SF_6 concentrations(C) were compared for these profiles using different grid sizes. As illustrated in **Fig. 6**, the setup features perpendicular lines—L1, L2, and L3—positioned precisely at the midpoint of each respective room, while perpendicular lines L4, L5, and L6 are strategically situated at the canyon's street midpoint, dividing it evenly.

Table 3 shows the average GCI for the three mesh types for perpendicular lines L1, L2, L3, L4, L5, and L6. The results indicates that the indoor flow field is more sensitive to the resolution of the unistructural mesh than the outdoor. For indoor wind speed distribution, the largest GCI discrepancy between the medium and coarse grids on L3 is 5.18%. The GCI discrepancies between the medium and fine grids are all less than 3%. For outdoor wind speed distribution, the largest GCI discrepancy between the medium and coarse grids on L5 is 2.21%. The GCI discrepancies between the medium and fine grids are all less than 3%. The findings reveal that differences in the vertical concentration distributions across the three grids are insignificant for both indoor and outdoor environments. However, a noteworthy distinction emerges in the indoor vertical velocity distribution when comparing the coarse and medium grids. In light of these results, a medium grid configuration is adopted for this study, striking a compromise between computational accuracy and efficiency.

2.6 Validation of CFD methodology

The turbulence model, pressure-velocity coupling method, and discretization schemes employed in this study are identical to those described in the previous work [36], as summarized in Table 1. In the authors' previous study [36], model validation was conducted by quantitatively comparing velocity profiles at three distinct vertical locations, x = 1.07H, 1.125H, and 1.25H, on the plane y = 0. The simulation results showed good agreement with the velocity measurements from the WTE. Although the CFD simulations exhibit a slight underestimation of the Strouhal number (St) in terms of ventilation frequency, this deviation, which is approximately 18% and consistently observed in other related studies [33], does not undermine the primary conclusions of the research; hence, such a degree of discrepancy is deemed acceptable. Moreover, the prediction of the ventilation rate reveals an error margin of around 7.9%.

Additionally, the accuracy of the simulation in ventilating street canyons has also been validated. The data analyzing pollutant dispersion in the outdoor domain of street canyons are sourced from the CODASC database [34]. The 1.2 m long model street canyon was formed by two parallel building blocks, each with a height of 120 mm and a depth of 120 mm. These blocks were positioned apart to create a street of width 120 mm, as shown in **Fig. 7(a)**. SF_6 tracer gas was released within the street canyon. SF_6 concentrations were measured at the canyon walls and the normalization is carried out according to Eqn. (5). More information about same is available online [34].

$$C^* = \frac{C*H*U_{ref}}{Q/l} \tag{5}$$

where C represents the average concentration level obtained from measurements, U_{ref} signifies the velocity of the wind measured at a predetermined reference height, H. Q/l characterizes the intensity of emissions per unit length of the emitting source.

Fig. 7(b) illustrates the CFD model and WTE normalized concentration of the tracer gas along the street walls. To quantitatively assess the congruence between the CFD outcomes and WTE data, a suite of validation metrics is employed, comprising Fraction Bias (FB), Normalized Mean Square Error (NMSE), Normalized Absolute Difference (NAD), and Fraction Within a Factor of Two (FAC2). These metrics' calculated values are categorized using a predefined membership function based on their ranges. Broadly, the concentration profiles derived from both CFD simulations and WTE align satisfactorily, as evidenced in Table 4, reflecting a good level of agreement.

2.7 Ventilation indices

The ventilation rate in a single-sided system has two components: the mean and fluctuating components. The mean ventilation rate, denoted $\bar{Q}_{raw}$ signifies the average value calculated from instantaneous ventilation rates over time. Instantaneous ventilation rate, Q_{raw} refers specifically to the volume of air that passes through every opening at any given moment. Given the principle of mass conservation, it's assumed that the volume of air flowing through both openings is equal. The fluctuating component $\sigma_{Q_{raw}}$ can be interpreted as the root mean square (RMS) deviation of Q_{raw}, representing a quantification of the variability in the instantaneous ventilation rate about its mean value, expressed as:

$$\sigma_{Q_{raw}} = \left[\frac{1}{N}\sum_1^N (Q_{raw} - \bar{Q}_{raw})^2\right]^{\frac{1}{2}} \tag{6}$$

where N denotes the number of recorded Q_{raw}.

The total ventilation rate $Q_{b_{raw}}$ is the superposition of the mean and fluctuating components [35]. $Q_{b_{raw}}$ of SSV is thus given as

$$Q_{b_{raw}} = \overline{Q_{raw}}(1 + \frac{2\sqrt{2}}{\pi}(\frac{\sigma_{Q_{raw}}}{\overline{Q_{raw}}})\sqrt{1 - \frac{1}{2}(\frac{\overline{Q_{raw}}}{\sigma_{Q_{raw}}})^2} \quad (7)$$

The mean and fluctuating ventilation rates are standardized using the following approach:

$$\bar{Q} = \frac{\bar{Q}_{raw}}{U_{ref}A_{ref}} \quad (8)$$

$$\sigma_Q = \frac{\sigma_{Q_{raw}}}{U_{ref}A_{ref}} \quad (9)$$

$$Q_b = \frac{Q_{b_{raw}}}{U_{ref}A_{ref}} \quad (10)$$

$$A_{ref} = \frac{A_1A_2}{\sqrt{A_1^2+A_2^2}} = \frac{A}{\sqrt{2}} \quad (11)$$

where U_{ref} denotes the reference velocity. $\bar{Q}$, σ_Q and Q_b represents the dimensionless quantities for the mean, fluctuating, and total ventilation rates. A_{ref} represents the effective area of room openings and A denotes the area of each opening [6].

3. Results and discussion

3.1 Single and multi-unit buildings

This study first contrasted the single and multi-unit buildings by analyzing the simulation results of case A-0 and case B-0. The normalized total, mean and fluctuating ventilation rates for diverse room (i.e. RB~RI and single-unit) have been presented in Fig. 8. Considering the potential impact of side vortex effects, neither RA nor RJ rooms were taken into account. Generally, normalized total ventilation rate Q_b has the highest value (= 0.217) when the room positions are in RE and RF. According to the symmetrical distribution of rooms within the building, the ventilation characteristics of rooms RB~RE are consistent with those of rooms RF~RI; Consequently, the result analysis focuses only on the ventilation performance of rooms RB~RE. Q_b has a monotonic variation with room position. It decreases from 0.217 (RE) to 0.081 (RD) and then to 0.072 (RC), and finally to 0.041 (RB). Q_b decreases by 54% from room RE to RD, by 28% from RD to RC, and by 43% from RC to RB. These results suggest that the ventilation efficiency of SS2 is greatly decrease when the room position is close to the middle room (RE), whereas it is less reduced when the room position is far from the middle room. The variation of the dimensionless mean ventilation rate $\bar{Q}$ and the dimensionless fluctuating ventilation rate σ_Q with room position resembles that of Q_b, decreasing gradually with room positions moving from RD to RB and experiencing a sharp decline from RE to RD. On other side, for the ventilation rate of the single-unit condition (case A-0), Q_b is only 67.07% compared to RB in Case B-0, or 12.67% relative to that of RE. It suggests that the ventilation rates in multi-unit buildings are greatly higher than single-unit building. Indicating the potential for enhancing the single-sided ventilation rate of multi-unit buildings. The increase in ventilation rates in the multi-unit could be attributed to the much larger negative pressure area in the wake vortex region, which leads to much higher wind velocity and turbulence fluctuation energy.

To delve further into ventilation characteristics, the differential pressure coefficients between rooms with two openings in Case A-0 and different rooms of Case B-0 are compared. **Fig. 9** illustrates the time series of the instantaneous pressure coefficient difference between two openings $\Delta C_p = \frac{p_1 - p_2}{\frac{1}{2}\rho_a U_{ref}}$. p_1 and p_2 are the instantaneous static pressure over the surfaces of each opening. ρ_a is the ambient air density. The time series of ΔC_p overall shows periodic sinusoidal variation around $\Delta C_p = 0$ for the single-unit case (Case A-0), indicating that the airflow velocity and orientation both change periodically. For the multi-unit case (Case B-0), the time series of ΔC_p indicates that variations of ΔC_p in each room of Case B-0 are not as regular as that of Case A-0 and has consistently negative values. It indicates that the wind direction is not changed. The mean pressure coefficient $\overline{\Delta C_p}$ has the minimum value for RB, which is still larger than that of Case A-0. From RB to RE, the $\overline{\Delta C_p}$ progressively increases and reaches the maximum at RE (=0.0265). From **Fig. 8**, it can be seen that for both single-unit and multi-unit buildings, the contribution of mean and fluctuating components to the total ventilation rate is almost the same. Therefore, $\sigma_{\Delta Cp}$ is not negligible any more in these conditions. The variation of pressure coefficient difference indicates that, compared to single-unit condition, multi-unit condition enhances SS2 ventilation performance, with the middle room showing the best ventilation performance.

Fig. 10 shows the top view of the three-dimensional time-averaged flow field and wind speed ratio distribution inside and outside the building. The lee vortex is prominent in multi-unit configuration, as depicted in Fig. 10(a). This results in the jets adhering closely to the leeward side of the building, accompanied by a noticeable rise in the ventilation rate (Fig. 8), especially in room RE and RF. From the perspective of mean flow fields, after fluid flows around a building, two vortices of equal size but opposite rotation directions form on the leeward side of the building. At the point where these two vortices intersect, there is a synergistic effect on the velocity at the center, leading to a significant increase in flow velocity at the central location on the leeward side of the building. Consequently, the ventilation rate in the room located at this position (referred to as the RE room) is greater than that in other rooms. Additionally, the larger vortices cause changes in the direction of airflow entering the indoor spaces, with the airflow direction at the window of room RE being more conducive to air exchange. On rooms RE to RB, the decrease in the angle between the airflow direction and the opening is observed (Fig. 10(b)–(e)), resulting in a gradual decrease in the ventilation rate.

SS2 of single-unit was firstly identified by Daish et al. [6]. It is induced by periodic vortex shedding and sinusoidal variation of ventilation rate time history can be observed at the opening [36]. Therefore, the power spectrum density (*PSD*) distribution for room of multi-unit should be obtained via performing fast Fourier transformation (FFT) on the time series of Q_{raw}, shown in Fig. 11. PSD_{max} is an important metric that describes the frequency domain energy distribution of instantaneous ventilation rates. It can be observed that PSD_{max} generally increases as the room location closer to the center of the building, implying that the peak turbulence fluctuating energy gradually strengthens from RB to RE. Accordingly, the dimensionless fluctuating airflow rate increase gradually (**Fig. 8**). In addition, the dominant frequency shows negligible variation among different rooms, suggesting that the ventilation frequency is independent of the room location. However, the frequency (f) of Case B-0(0.4*Hz*) is considerably lower than that of Case A-0 (1.7 *Hz*). Based on the Strouhal number (St)=$\frac{fL}{U_{ref}}$, since St and reference wind speed U_{ref} remain constant, a larger characteristic length L of a broader building results in a reduction of the frequency f.

3.2 Impact of the T-shaped street intersection

In this section, the influence of the T-shaped street intersection on the ventilation performance of the multi-unit SS2 under different wind directions is investigated (Case C in **Fig. 3**). To make a comparison with that in Case B without intersection. Distribution contour of dimensionless mean and fluctuating ventilation rate ($\bar{Q}$ and σ_Q) obtained for Case B and Case C at different wind directions are shown in **Fig. 12**. The rules of change in the dimensionless fluctuating ventilation rate σ_Q are consistent with the dimensionless mean ventilation rate $\bar{Q}$. It can be found that the rooms with the most prominent ventilation rates are RE, RF, and RI. In Case B at different wind direction, the maximum $\bar{Q}$ appears in Case B-90, reaching 0.17. It's worth noting that the lowest $\bar{Q}$ also occurs at Case B-90, which is only 0.00045. This indicates that the distribution of ventilation rate is extremely uneven in these cases. Compared to Case B, the $\bar{Q}$ for Case C are generally improved across the board, with the lowest $\bar{Q}$ of 0.002 at Case C-90. In all the cases investigated, the maximum $\bar{Q}$ appears in Case C-180, the $\bar{Q}$ of the Case C-180 is about 1.4 times that of the Case B-90.

Fig. 13 illustrates the variations in ventilation rates between Case B and Case C, from room RB to room RI, under different wind orientations. Overall, T-shaped intersections have the potential to enhance ventilation efficiency. This conclusion is consistent with the findings of Guo et al.'s research [37]. Overall, the dimensionless mean ventilation rate $\bar{Q}$ show the most significant increases under Conditions C-135 and C-90. Particularly, the dimensionless mean ventilation rate $\bar{Q}$ in the RD room under Case C-135 shows the most significant increase, being approximately 135 times higher than that under Case B-135. But the dimensionless mean ventilation rate $\bar{Q}$ may also be reduced in inappropriate circumstances: for example, Cases C-0 and 45 exhibit an overall declining trend, with maximum decreases of 0.87 times and 0.93 times, respectively. Finally, the dimensionless mean ventilation rate $\bar{Q}$ of T-shaped street intersection is so good as (by -0.9 times to 135 times) those of the reference Case B, which may be due to the T-shaped street intersection increasing the effective negative pressure zone around the building.

As regards Case C, to further explore the impact of street-level pollutants on indoor air quality, with a focus on the pollutant distribution of indoor zone, as shown in **Fig. 14**. It can be observed that, on average, the pollutant concentration of indoor is larger for the wind directions φ = 0°, 45°, and 90°, and a large extent of high concentration areas exist within the T-shaped street intersection (C approximately equal to 0.01ppm). When φ = 135° and 180°, the pollutant concentration is relatively lower at the indoor. Specifically, the airflow distribution tends to flow more easily within the T-shaped street intersection, with no evident accumulation of pollutants. Overall, the pollutant concentration gradually decreases indoors and within the canyon as the wind direction(φ) shifts from 0 to 180°, it demonstrates that Case C-180 exhibits superior overall ventilation performance compared to other cases. Finally, considering **Fig. 12**, the indoor ventilation rate is not always positively correlated with the distribution of pollutant concentrations, with a marked difference between the different wind directions.

Fig. 15(a) shows the average values of the dimensionless total ventilation rate Q_b and the normalized pollutant concentration C^* in all room with multi-unit for the different wind directions, with indication of the average values of each case, as well as the maximum values. The data for wind directions at 225°, 270°, and 315° are copied from the symmetric cases. When the wind direction is at 0° and 180°, the average value of total ventilation rates Q_b are relatively higher. This indicates that wind directions perpendicular to the building orientation favor the exchange of air between indoor and outdoor environments, thereby enhancing ventilation. In the Case C, the one with the maximum Q_b at the indoor part is Case C-180, reaching 0.3, followed by Case C-0 and Case C-90(270), reaching 0.25 and 0.2, respectively. Case C-45 with the lowest average total ventilation rate Q_b, merely 0.05. The maximum of the Case C-180 is about 6 times that of the Case C-45(315). The case with the lowest pollutant concentration C^* is Case C-180, with a value of 0.11. The highest concentration C^* is found in Case B-90(270), with a value of 2.96, indicates that the impact of wind direction on the ventilation performance of multi-unit buildings is significant.

In addition, there is considerable variation in ventilation performance among different rooms, shown in **Fig. 15(b)**. The average and maximum values of the dimensionless total ventilation rate Q_b and the normalized concentration C^* under all wind directions for different rooms. The maximum total ventilation rate Q_b appears in RE and RF, reaching 0.31, and the maximum C^* appears in RB, reaching 9.81. The average value of total ventilation rates for RE and RF are significantly higher than those of other Cases under the same conditions. The average value of pollutant concentrations for RB and RC are significantly higher than those of other cases under the same conditions. This indicates that the room location has a significant impact on ventilation performance, and there is no apparent relationship between ventilation rates and pollutant levels.

3.3 Impact of the T-shaped street intersection with CV

In this section, influence on CV of the multi-unit buildings by the T-shaped street intersection is investigated. **Fig. 16** compares the dimensionless mean ventilation rate $\bar{Q}$, the dimensionless fluctuating ventilation rate σ_Q and the normalized pollutant concentration C^* of each room at different wind direction for Case D. Overall, $\bar{Q}$ and σ_Q show the same trend with increase of wind direction in Case D. The influence of wind direction on the ventilation performance of multi-unit buildings is greater than that of room location. $\bar{Q}$ is significantly higher under a wind direction of 0° compared to other wind directions, and the pollutant concentration C^* is notably higher at a wind direction of 135°. At a wind direction of 0°, the dimensionless mean ventilation flow $\bar{Q}$ for RE and RF peaks at 0.77, while at a wind direction of 135°, the $\bar{Q}$ for RE is the lowest (decreasing to 0.0052). In contrast, $\bar{Q}$ on average increases by a factor of 147. This phenomenon may be attributed to variations in the negative pressure in the wake region caused by changes in wind direction, which leads to much higher wind velocity and turbulence fluctuation energy. However, the variations in normalized pollutant concentration C^* are not as consistent with $\bar{Q}$ and σ_Q. The pollutant concentrations for RC, RD, and RE stand out notably under a wind direction of 135°. The maximum pollutant concentration C^* for RE reaches 1.55. There are no significant variations in pollutant concentrations across other scenarios.

Fig. 17 illustrates the variations in ventilation rates and pollutant concentration between Case C and Case D, from room RB to room RI, under different wind orientations. Overall, the CV have the potential to improve the ventilation efficiency. For example, Case D-45 increases the ventilation rate value by 124 times, and reduces the C^* by 0.9 times; Case D-0 increases the ventilation rate value by 111 times and reduces the average C^* by 0.39 times. But the ventilation performance may also be reduced in inappropriate circumstances: for example, Case D-135 experiences a reduction of the ventilation rate value by 0.8 times, Case D-180 with a C^* value increased by 10 times. Finally, the ventilation of CV could be increased by −0.8 to 124 times compared with Case C. Compared to Case C, the pollutant concentration C^* is significantly reduced in most rooms, however, in some cases, indoor C^* increase by nearly 10 times. The ventilation efficiency of the CV system is significantly higher, which may be attributed to the optimized window layout of the CV, reducing the resistance of the ventilation airflow.

Fig. 18(a) shows the average values of the dimensionless total ventilation rate Q_b and the normalized pollutant concentration C^* in all room with multi-unit for the different wind directions, with indication of the average values of each case, as well as the maximum values. The data for wind directions at 225°, 270°, and 315° are copied from the symmetric cases. When wind directions is at 0° and 45°(315°), the average value of Q_b are relatively higher. This may be attributable to the location of the aperture in the windward aspect. In Case-D, the one with the maximum Q_b at the indoor part is Case D-0, reaching 0.99, followed by Case D-45(315) and Case D-180, reaching 0.62 and 0.32, respectively. Case D-135(215) with the lowest average value of Q_b, merely 0.064. The maximum of the Case D-0 is about 15.5 times that of the Case D-135. The case with the lowest pollutant concentration is Case D-0, with a value of 1.7e-6. The highest concentration is found in Case D-135, with a value of 0.4, indicates that the impact of CV on the ventilation performance of multi-unit buildings is significant.

The average and maximum values of the dimensionless total ventilation rate Q_b and the normalized concentration C^* under all wind directions for different rooms, shown in **Fig. 18(b)**. Case D show more even ventilation rate distribution, with no high pollutant concentration areas. In all the wind direction investigated, the maximum total ventilation rate appears in RD and RG, reaching 1.04, and the maximum C^* appears in RD(RG), reaching 1.55. The average total ventilation rates for RB and RI are slightly higher than those of other cases under the same conditions. Compared to Case C, Case D is more suitable for the ventilation of surrounding buildings at a T-shaped street intersection.

4. Limitations & future work

This study used CFD simulation based on URANS to investigate the effect of T-shaped street intersection on the ventilation performance and pollutant dispersion inside and outside the multi-unit building. The predictive accuracy may be inherently confined by the intrinsic shortcomings of URANS in capturing turbulent fluctuations to a certain extent. In future studies, methods such as Large Eddy Simulation (LES) and WTEs will be adopted to thoroughly investigate the turbulent characteristics and the transmission mechanisms of indoor and outdoor contaminants within multi-unit buildings. Additionally, in complex urban environment, investigating the natural ventilation performance of street-surrounding buildings by considering only wind direction may not be insufficient. Therefore, future studies will consider the micro-climates (including local wind speed, temperature, humidity, etc.) in urban areas to investigate the airflow and concentration fields in the street canyons. Future research will further investigate the different dispersion characteristics of traffic pollutants on various floors and within the street environment.

5. Conclusions

This paper studied the natural ventilation performance and pollutant dispersion inside and outside the multi-unit buildings at T-shaped street intersection. Investigated the differences in SS2 ventilation performance between multi-unit and single-unit building, as well as the impact of T-shaped street intersections on the natural ventilation of surrounding structures. Main conclusions are as follows:

(1) Multi-unit buildings have the potential to enhance the SS2 ventilation performance. Compared to single-unit buildings, the ventilation rate of the centrally located room (RE) in multi-unit buildings increases significantly, reaching 135 times that of single-unit buildings. The ventilation rate of rooms located on the sides of the building is 1.7 times lower than that of centrally positioned rooms, but it remains higher than the ventilation rate in single-unit buildings. This may be due to the synergistic effect of vortices at the center of the leeward side of multi-unit buildings, which leads to an increase in flow velocity, thereby enhancing SSV. Compared to single-unit building, the pressure coefficients for each room in multi-unit buildings do not exhibit a clear periodicity, but they all show enhancement to a certain extent. Additionally, the ventilation frequency for each room in the multi-space buildings remains consistent at 0.4 Hz.

(2) The T-shaped intersection have the potential to enhance the ventilation rate. In contrast, the dimensionless mean ventilation rate $\bar{Q}$ of T-shaped street intersection could be increased by -0.9 to 135 times compared with Case B. Among these, the ventilation rates of rooms located centrally and at the ends of multi-unit buildings

are relatively higher, possibly because these rooms are adjacent to airflow channels where the outdoor wind speeds are greater, thus facilitating ventilation. Additionally, the concentrations of pollutants indoors and outdoors are significantly related to the wind direction (φ). When the wind direction is at 180°, it is most conducive to the dilution of pollutants in the outdoor streets. Statistical analysis has shown that for multi-unit SS2 buildings, a wind direction of 180° is most favorable for overall ventilation performance. Among all the rooms, those located centrally in the building exhibit the best ventilation performance.

(3) The CV have the potential to boost the ventilation rate. Compared to Case C, the ventilation of CV could be increased by −0.8 to 124 times. The pollutant concentration C^* is significantly reduced in most rooms, however, in Case-135, indoor C^* increase by nearly 10 times. The maximum Q_b is 0.77, and the maximum C^* is merely 1.5. Overall, the CV performs better in the context of building ventilation within T-shaped street intersection compared to SS2. Unlike Case C, a 0° wind direction is more advantageous for enhancing ventilation in multi-unit buildings designed for CV, with rooms located at the sides of the building exhibiting the best ventilation performance.

Credit authorship contribution statement

Meng-Ying Chen: Writing – original draft, Methodology, Investigation, Formal analysis, Conceptualization. Jie Sun: Visualization, Validation, Software, Data curation. Huai-Yu Zhong: Formal analysis, Supervision, Writing – review & editing. Ya-Nan Liu: Methodology, Formal analysis, Conceptualization, Writing – review & editing. Wei Dong: Formal analysis, Supervision, Writing – review & editing. Yang Cai: Software, Validation. Fu-Yun Zhao: Methodology, Writing – review & editing. Fu-Ping Qian: Formal analysis, Methodology, Validation. Carlos Jimenez-Bescos: Formal analysis, Methodology, Writing – review & editing.

Data availability statement

The authors confirm that the data supporting the findings of this study are available within the article and its supplementary materials.

Disclosure statement

The authors declare that they have no known competing financial interests or personal relationships that could have appeared to influence the work reported in this paper.

Acknowledgements

Authors would gratefully acknowledge the financial supports of the *Natural Science Foundation of the Anhui Higher Education Institutions of China* (2022AH050307), *the Opening Fund of State Key Laboratory of Green Building in Western China* (LSKF202312), the National Natural Science Foundation (52208095) and the Chongqing Municipal Education Commission Science and Technology Project (KJQN202100736).

References

[1] P. L. Jenkins, T. J. Phillips, E. J. Mulberg, S. P. Hui. Activity patterns of Californians: Use of and proximity to indoor pollutant sources, Atmospheric Environment 26 (1992), 2141-2148.

[2] L. Pérez-Lombard, J. rtiz, C. Pout. A review on buildings energy consumption information. Energy and Buildings, 40(2008), 394–398.

[3] T. Abergel, et al. Energy Technology Perspectives 2017: Catalysing Energy Technology Transformations, OECD, 2017.

[4] T. Luo, Y. Tan, C. Langston, et al. Mapping the knowledge roadmap of low carbon building: A scientometric analysis. Energy and Buildings, 194 (2019), 163–176.

[5] H.-Y. Zhong, Y. Sun, J. Shang, et al. Single-sided natural ventilation in buildings: A critical literature review. Building and Environment, 212(2022), 108797.

[6] N. C. Daish, G. Carrilho da Graça, P. F. Linden, D. Banks. Impact of aperture separation on wind-driven single-sided natural ventilation, Build. Environ. 108 (2016), 122–134.

[7] G. Carrilho da Graça, P. Linden. Ten questions about natural ventilation of nondomestic buildings, Build. Environ. 107 (2016), 263–273.

[8] D. Albuquerque, M. Sandberg, P. Linden, G. Carrilho da Graça. Experimental and numerical investigation of pumping ventilation on the leeward side of a cubic building, Build. Environ. 179 (2020), 106897.

[9] C.-R. Chu, R.-H. Chen, J.-W. Chen. A laboratory experiment of shear-induced

natural ventilation, Energy Build. 43 (2011), 2631–2637.

[10] Z. T. Ai, C. M. Mak. Analysis of fluctuating characteristics of wind-induced airflow through a single opening using LES modeling and the tracer gas technique, Build.Environ. 80 (2014), 249-258.

[11] J. Park, X. Sun, J. Choi, G. Rhee. Effect of wind and buoyancy interaction on single-sided ventilation in a building, J. Wind Eng. Ind. Aerod. 171 (2017), 380–389.

[12] H. Zhong, Y. Jing, Y. Sun, H. Kikumoto, F. Zhao, Y. Li. Wind-driven pumping flow ventilation of highrise buildings: effects of upstream building arrangements and opening area ratios, Sci. Total Environ. 722 (2020), 137924.

[13] H.-Y. Zhong, J. Sun, C. Lin, S.-H. Wu, J. Shang, H. Kikumoto, F.-P. Qian, C. Jimenez-Bescos, F.-Y. Zhao. CFD simulation of pumping ventilation in a threestory isolated building with internal partitioning: effects of partition widths, heights and locations, Build. Simulat. 17 (2024), 267–284.

[14] Z. T. Ai, C. M. Mak. A study of interunit dispersion around multistory buildings with single-sided ventilation under different wind directions, Atmospheric Environment 88 (2014), 1-13.

[15] Z. T. Ai, C. M. Mak. Determination of single-sided ventilation rates in multistory buildings: Evaluation of methods, Energy and Buildings 69 (2014), 292-300.

[16] W. Pan, S. Liu, S. Li, X. Cheng, H. Zhang, Z. Long, T. Zhang, Q. Chen. A model for calculating single-sided natural ventilation rate in an urban residential apartment, Building and Environment 147 (2019), 372-381.

[17] C. Chen, B. Zhao, C. J. Weschler. Indoor exposure to ’outdoor PM_{10}": assessing its influence on the relationship between PM_{10} and short-term mortality in U.S.Cities on JSTOR, Epidemiology 23 (6) (2012), 870-878.

[18] K. Ahmad, M. Khare, K. K. Chaudhry. Wind tunnel simulation studies on dispersion at urban street canyons and intersections—a review. Journal of Wind Engineering and Industrial Aerodynamics. 93 (2005), 697–717.

[19] H. W. Dou, T. Z. Ming, Z. T. Li, et al. Numerical simulation of pollutant dispersion characteristics in a three-dimensional urban traffic system. Atmospheric Pollution Research. 9 (2018), 735–746.

[20] X. Guo, B. Riccardo, Z. Gao, et al. On the effects of urban-like intersections on ventilation and pollutant dispersion. Building Simulation. 15 (2022), 419–433.

[21] L. Soulhac, V. Garbero, P. Salizzoni, et al. Flow and dispersion in street intersections. Atmospheric Environment. 43 (2009), 2981–2996.

[22] W. Tan, C. J. Li, K. Wang, et al. Dispersion of carbon dioxide plume in street canyons. Process Safety and Environmental Protection. 116 (2018), 235–242.

[23] J. L. Shen, Z. Gao, W. D. Ding, et al. An investigation on the effect of street morphology to ambient air quality using six real-world cases. Atmospheric Environment. 164 (2017), 85–101.

[24] S. Ghorui. CFD study of ventilation in a room maintained under negative-pressure to prevent airborne contamination. FOSSEE, IIT Bombay. 2020.

[25] Z. M. Tong, Y. J. Chen, A. Malkawi. Defining the Influence Region in neighborhood-scale CFD simulations for natural ventilation design. Applied

Energy. 182 (2016), 625–633.

[26] E. Cuce, F. Sher, H. Sadiq, et al. Sustainable ventilation strategies in buildings: CFD research. Sustainable Energy Technologies and Assessments. 36 (2019), 100540.

[27] R. N. Meroney, M. Pavageau, S. Rafailidis, et al. Study of line source characteristics for 2-D physical modelling of pollutant dispersion in street canyons. J Wind Eng Ind Aerodyn 62 (1996), 37–56.

[28] R. C. Hall. Dispersion of releases of hazardous materials in the vicinity of buildings: Phase II—CFD modelling. Contract Research Report. Suffolk UK: The Health and Safety Executive. 127 (1997).

[29] J. Franke, A. Hellsten, H. Schlünzen, B. Carissino. Best Practice Guideline for the CFD Simulation of Flows in the Urban Environment. Brussels: COST Office. 44 (2011), 419-427.

[30] F. R. Menter. Two-equation eddy-viscosity turbulence models for engineering applications, AIAA J. 32 (1994), 1598–1605.

[31] H.-Y. Zhong, C. Lin, Y. Sun, H. Kikumoto, R. Ooka, H.-L. Zhang, H. Hu, F.-Y. Zhao, C. Jimenez-Bescos. Boundary layer wind tunnel modeling experiments on pumping ventilation through a three-story reduce-scaled building with two openings, Build. Environ. 202 (2021), 108043.

[32] P. J. Roache. Quantification of uncertainty in computational fluid dynamics, Annu. Rev. Fluid Mech. 29 (1997), 123–160.

[33] S. Murakami, A. Mochida. On turbulent vortex shedding flow past 2D square cylinder predicted by CFD, J. Wind Eng. Ind. Aerod. 54/55 (1995), 191–211.

[34] CODASC (2008). Concentration Data of Street Canyons. Internet database. Karlsruhe Institute of Technology (KIT).

[35] Straw MP (2000). Computation and measurement of wind induced ventilation. PhD Thesis, University of Nottingham, UK.

[36] H. Y. Zhong, J. Sun, C. Lin, et al. CFD simulation of pumping ventilation with two asymmetrically arranged openings on the rear wall in a three-story isolated building. Building and Environment, 256 (2024), 111486.

[37] X. Guo, R. Buccolieri, Z. Gao, et al. On the effects of urban-like intersections on ventilation and pollutant dispersion. Building Simulation, 15 (2022), 419-433.

[38] Tominaga, Y., Stathopoulos, T., 2007. Turbulent Schmidt numbers for CFD analysis with various types of flow field. Atmos. Environ. 41, 8091-8099.

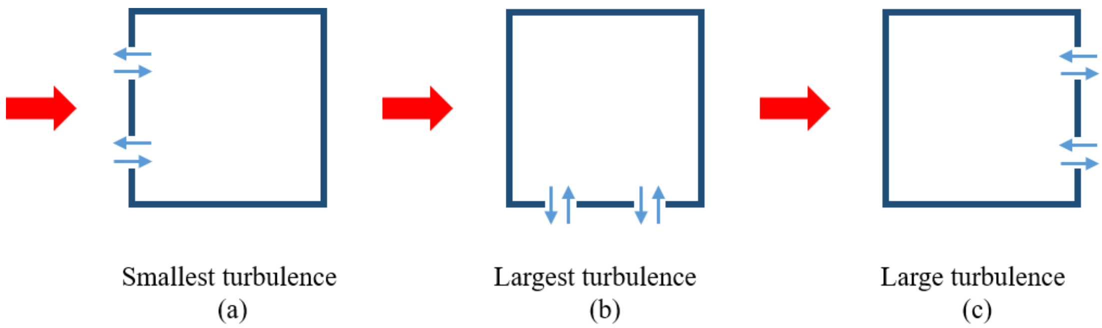

Fig. 1. Schemes of SS2 with different wind directions: (a) windward, (b) shear and (c) leeward ventilation.

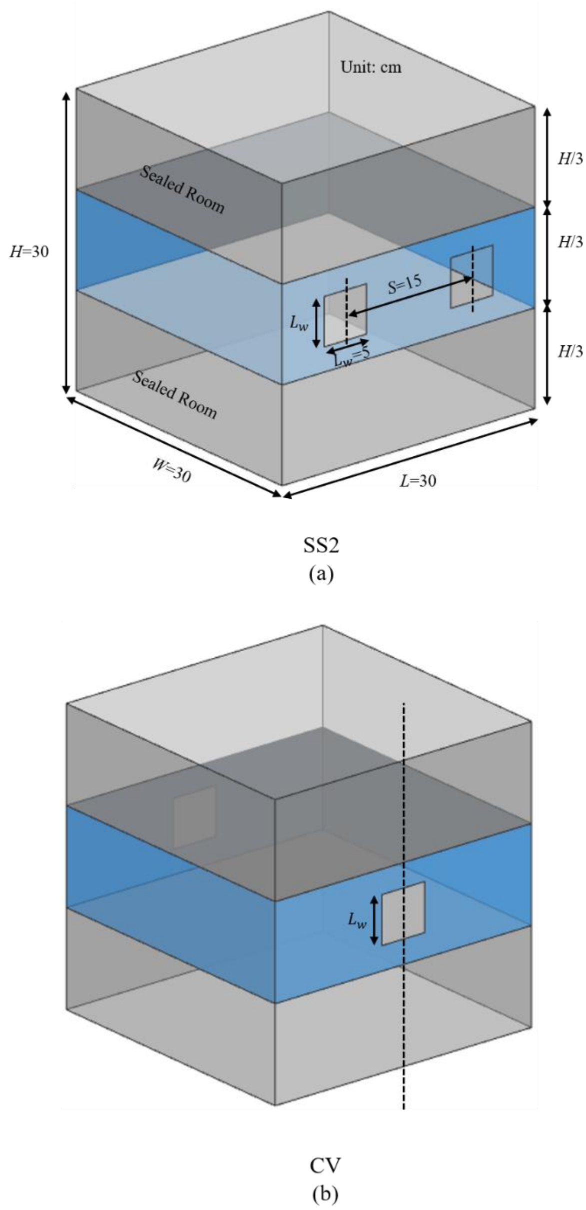

Fig. 2. Schematic diagram of the basic building model: (a)single-unit SS2 (b) single-unit CV.

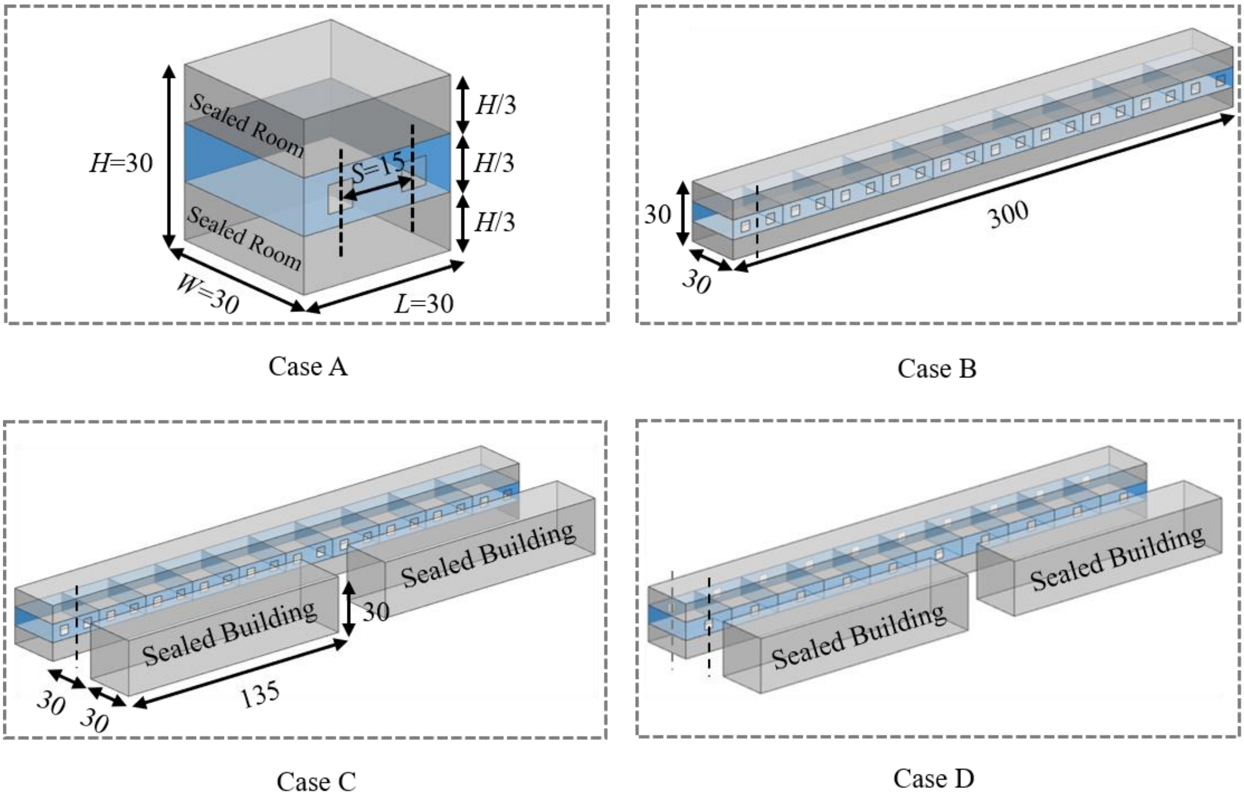

(a)

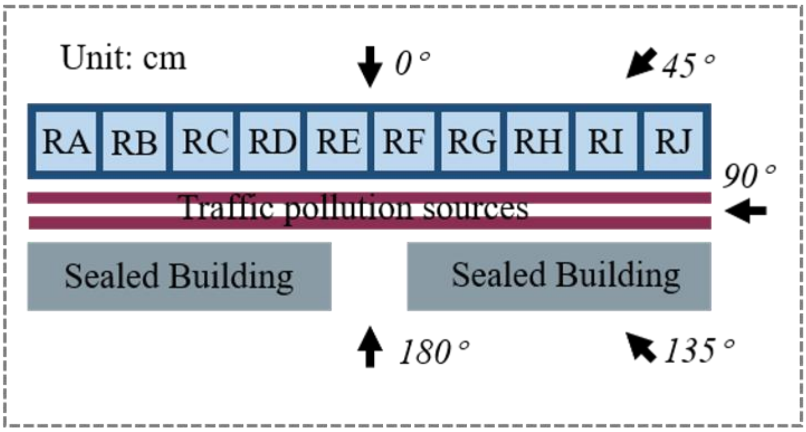

(b)

Fig. 3. Layout diagram of (a) building model configurations: Case A, Case B, Case C and Case D and (b) variation of incident wind direction.

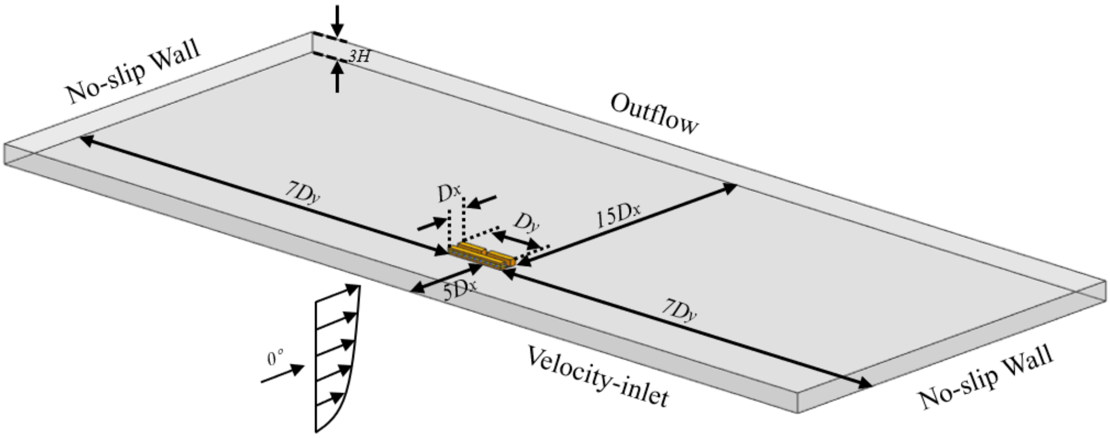

Fig. 4. Computational domain and boundary conditions.

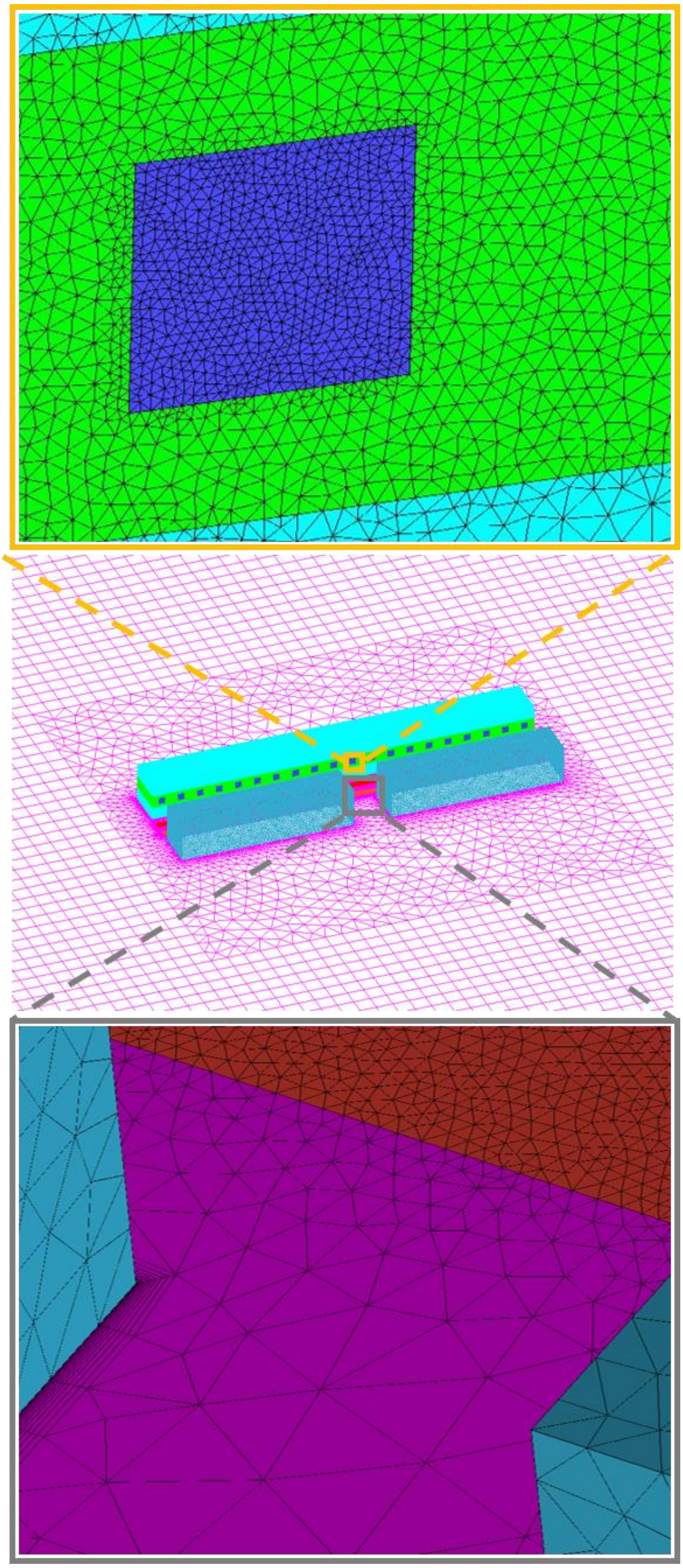

Fig. 5. Visual images of the grid constructed for the basic case.

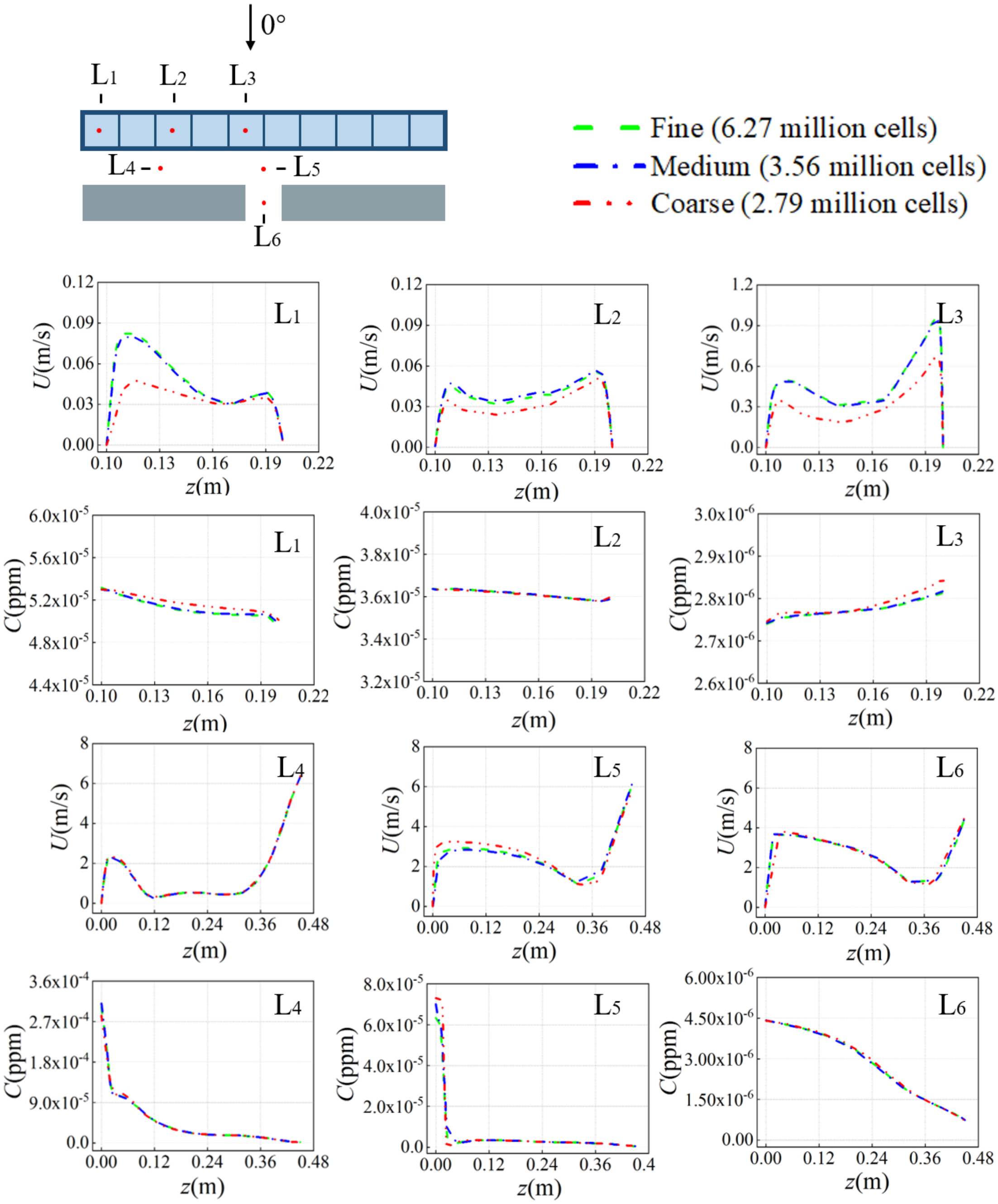

Fig. 6. Grid sensitivity analysis.

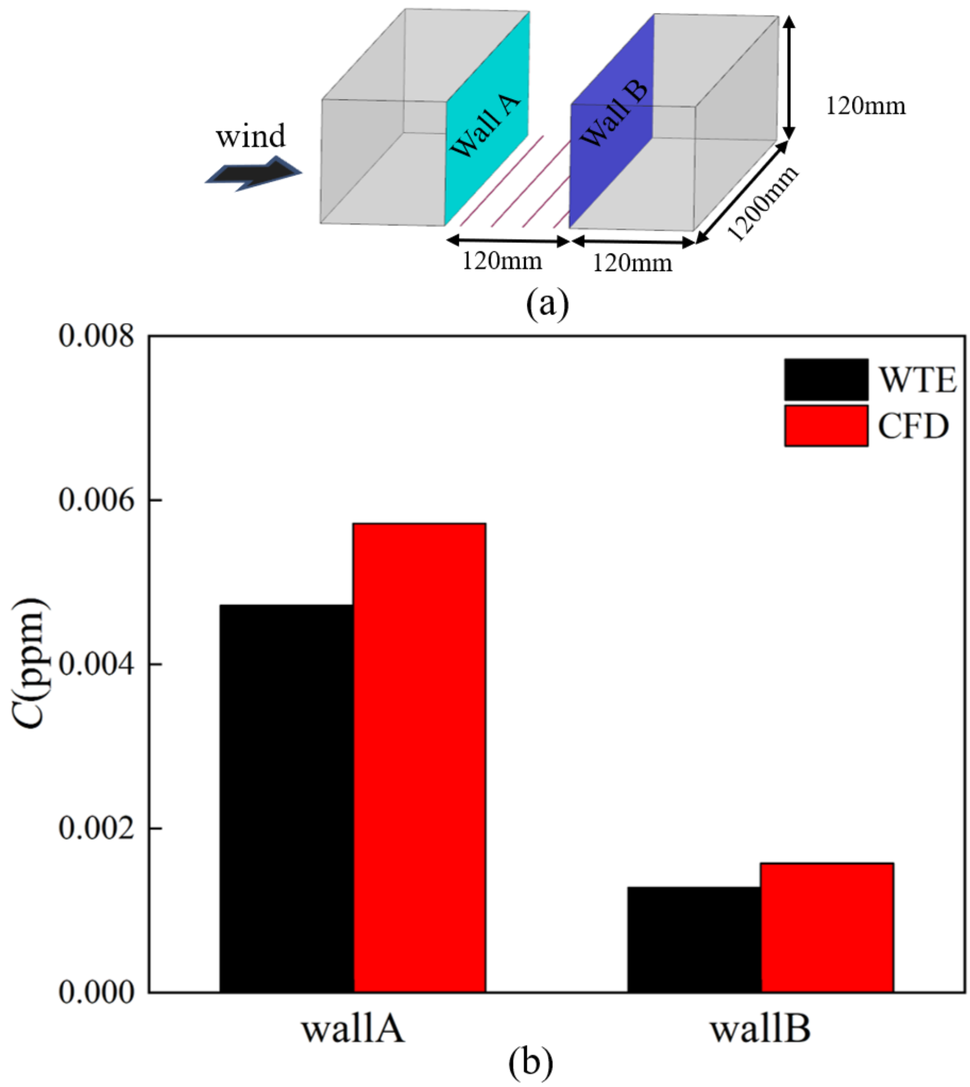

Fig. 7. Validation of simulation accuracy in ventilating street canyons: (a) building model in WTE [34], (b) comparison of the SF_6 concentration of street canyons for wall A and wall B.

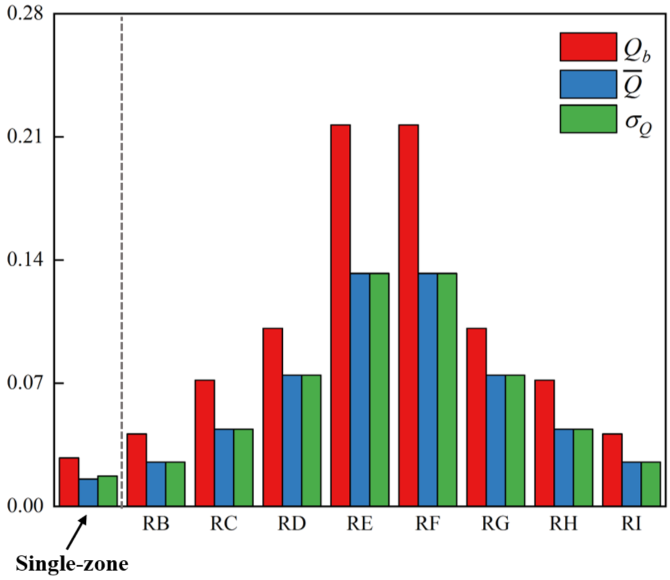

Fig. 8. The dimensionless ventilation rates of single-unit versus multi-unit configurations: $\bar{Q}$, σ_Q and Q_b are the dimensionless mean, fluctuating and total ventilation rate.

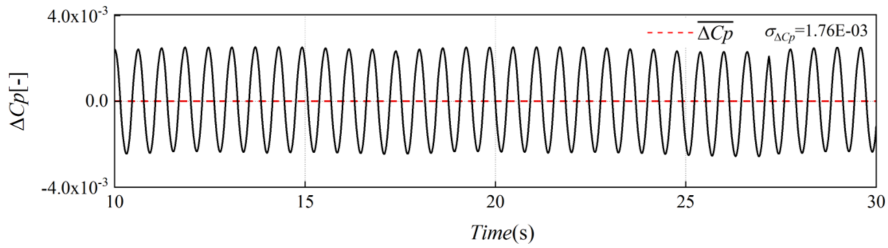

(a) single-zone

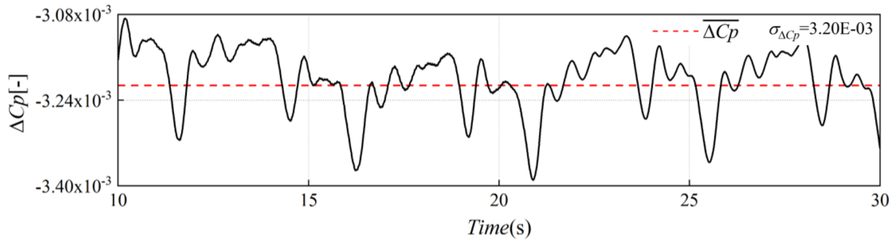

(b) RB

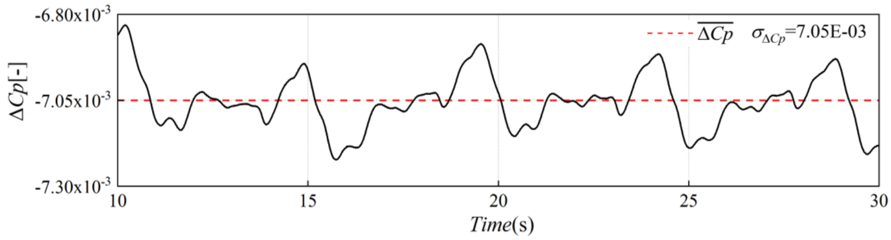

(c) RC

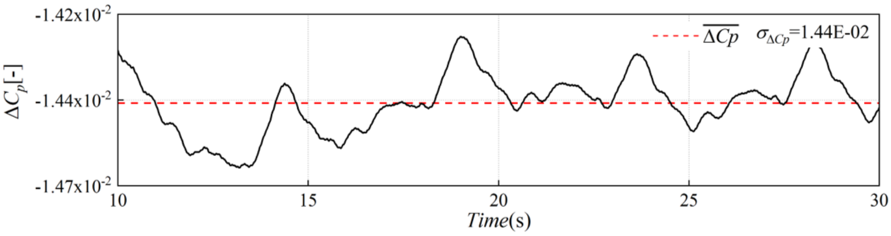

(d) RD

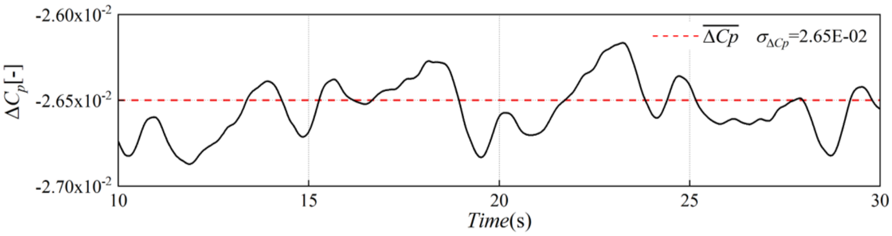

(e) RE

Fig. 9. The time series of ΔC_p of single-unit versus multi-unit configurations.

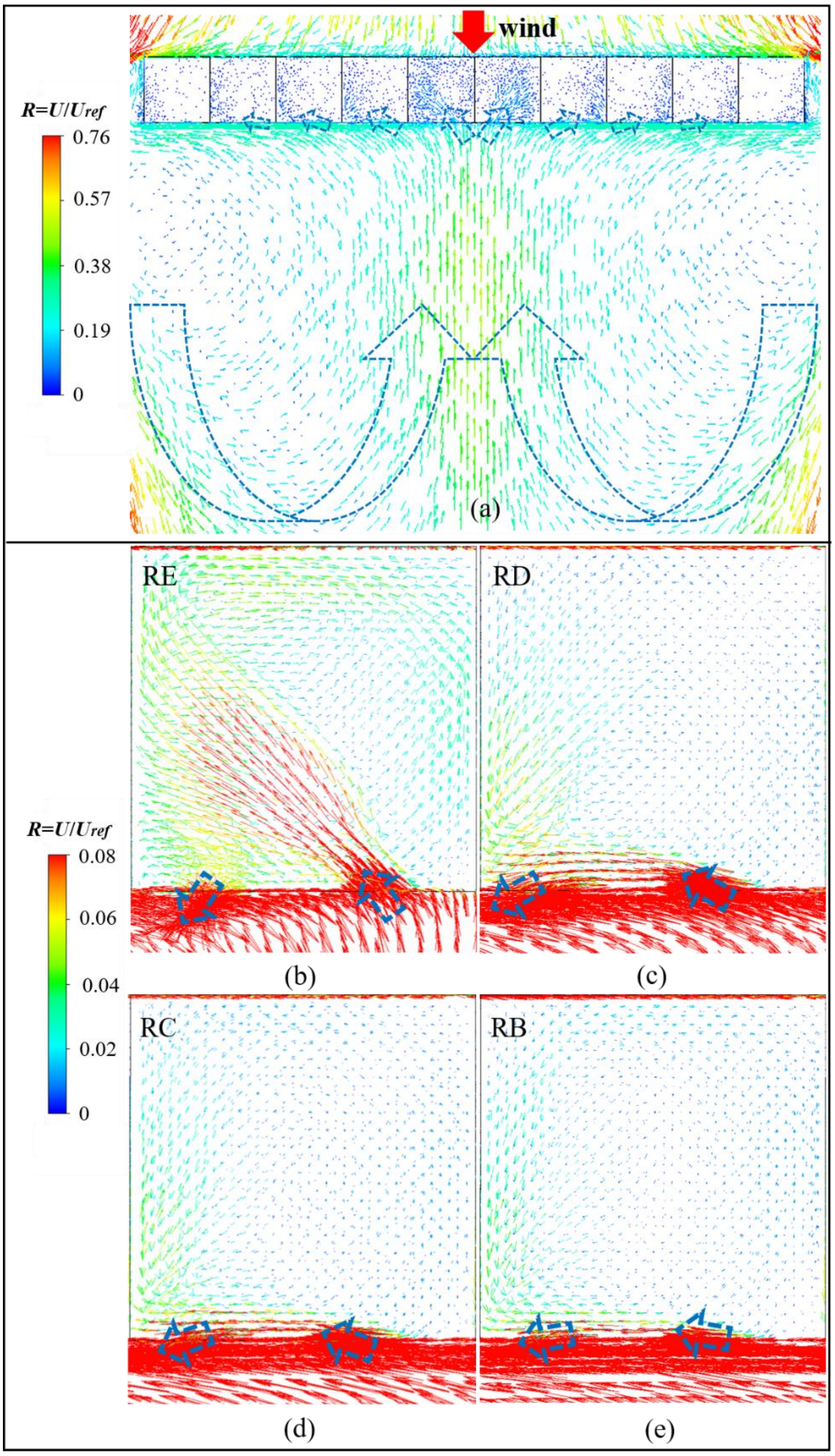

Fig. 10. Top view of the time-averaged velocity vectors for various room locations within the building.

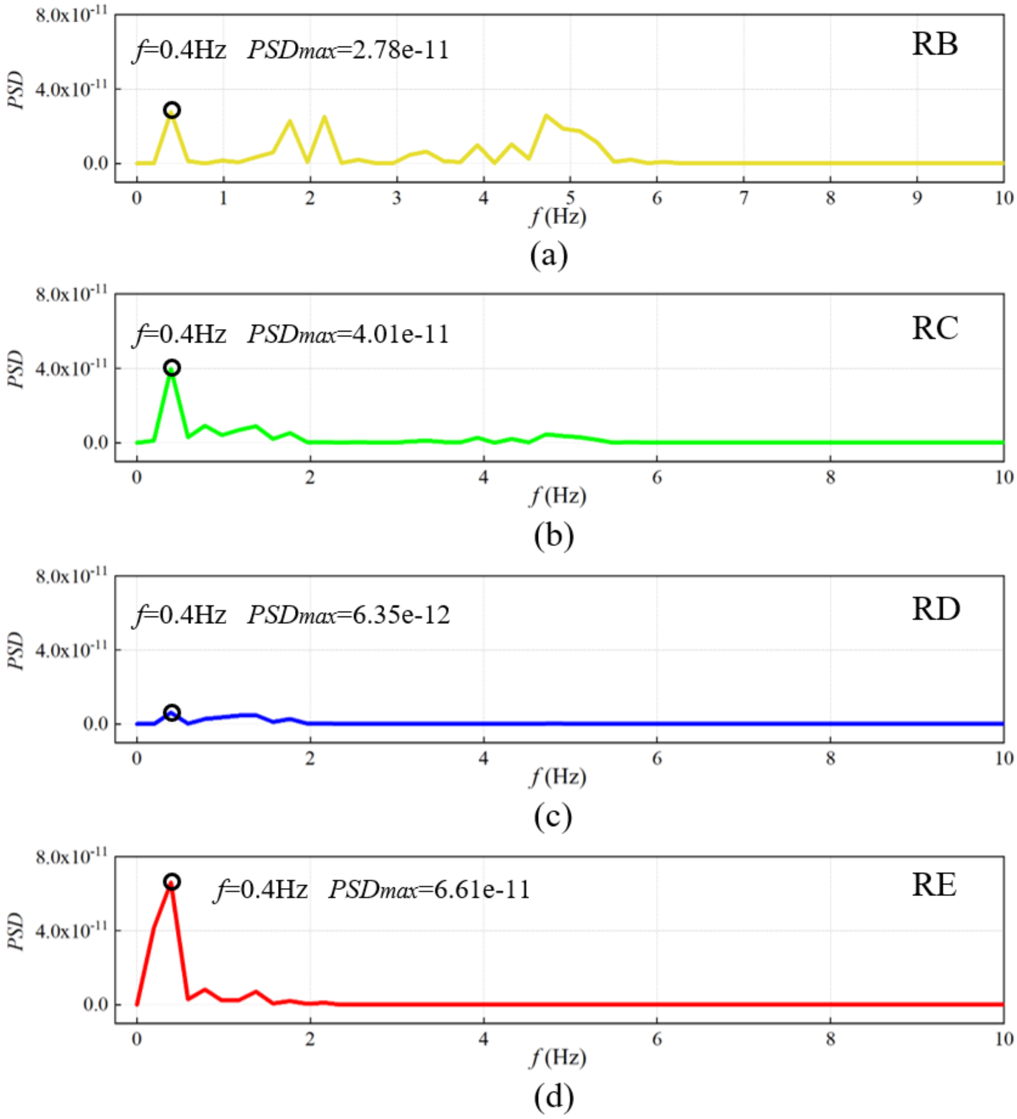

Fig. 11. Oscillation characteristics of SS2 ventilation for various room locations.

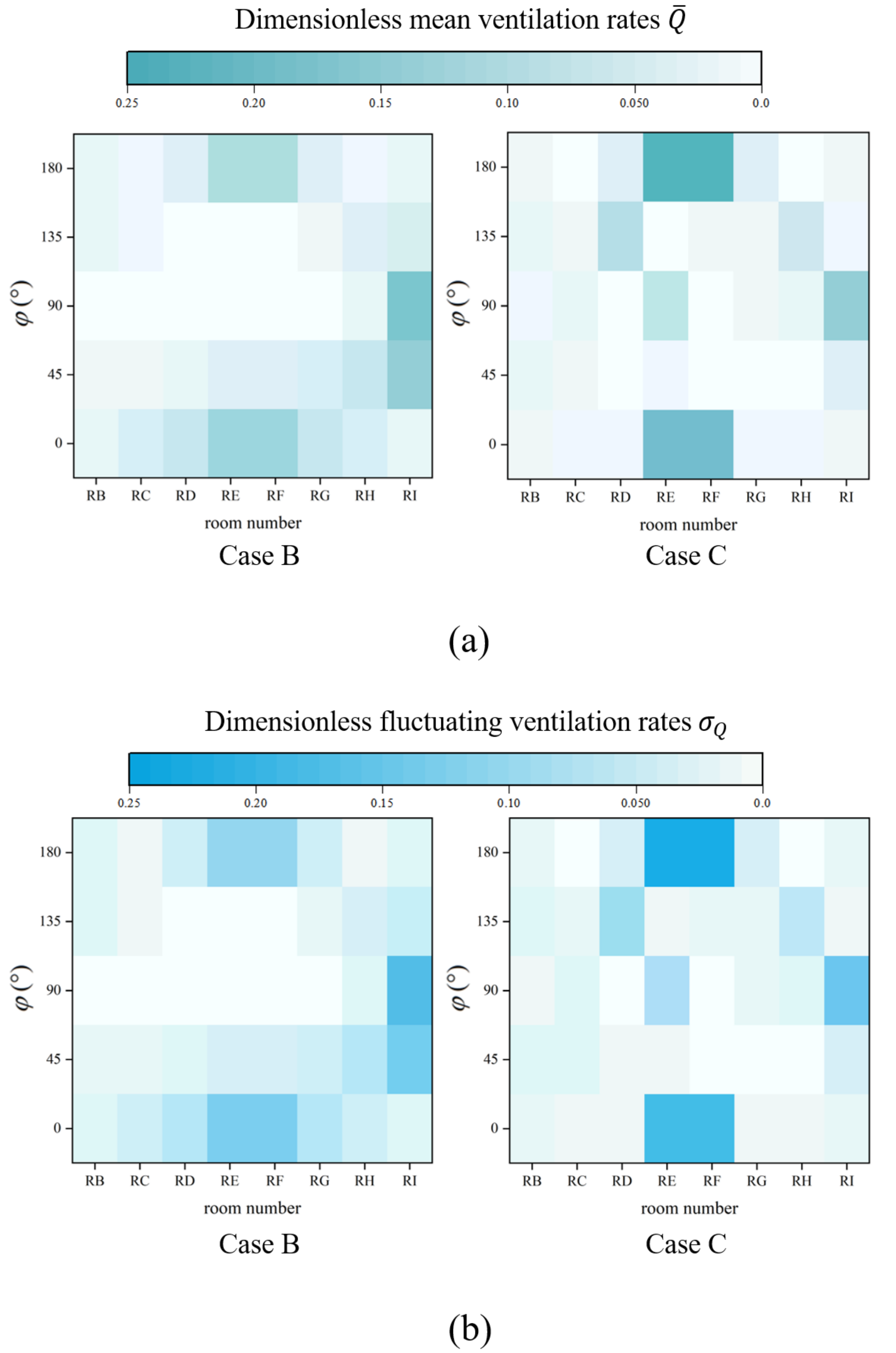

Fig. 12. The mean ventilation rates $\bar{Q}$ and fluctuating ventilation rates σ_Q for Case B and Case C under different wind directions.

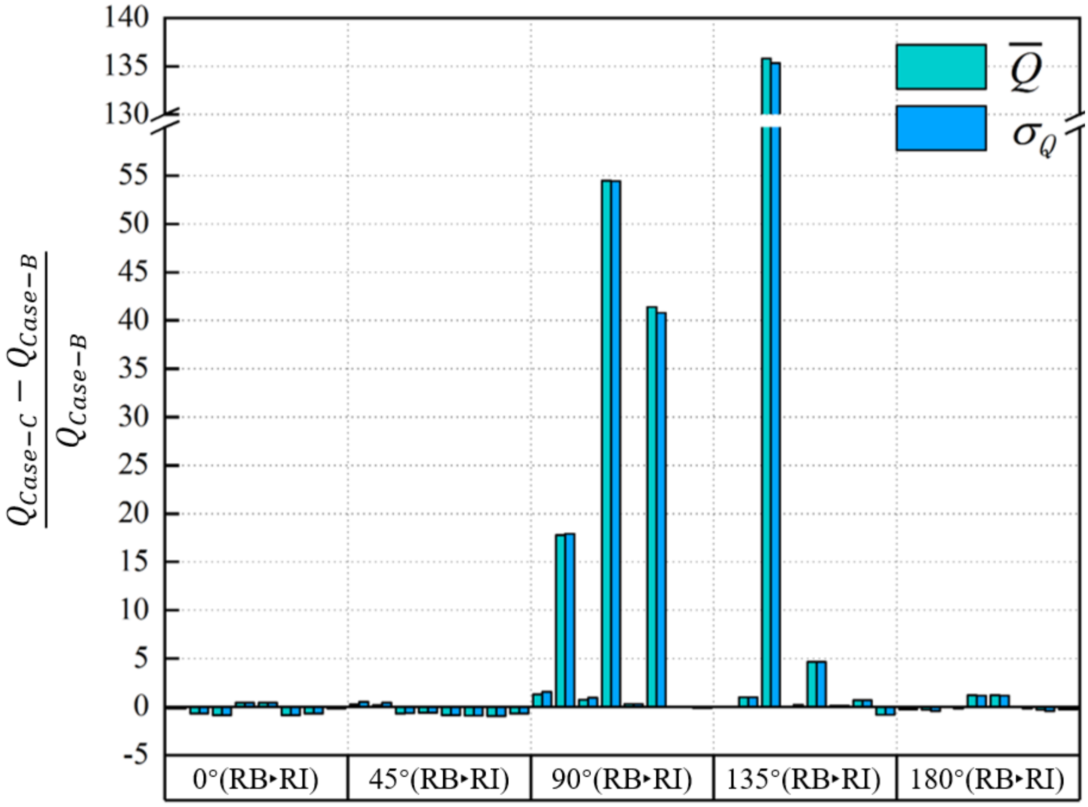

Fig. 13. Variation of the ventilation rate of Case C compared to Case B.

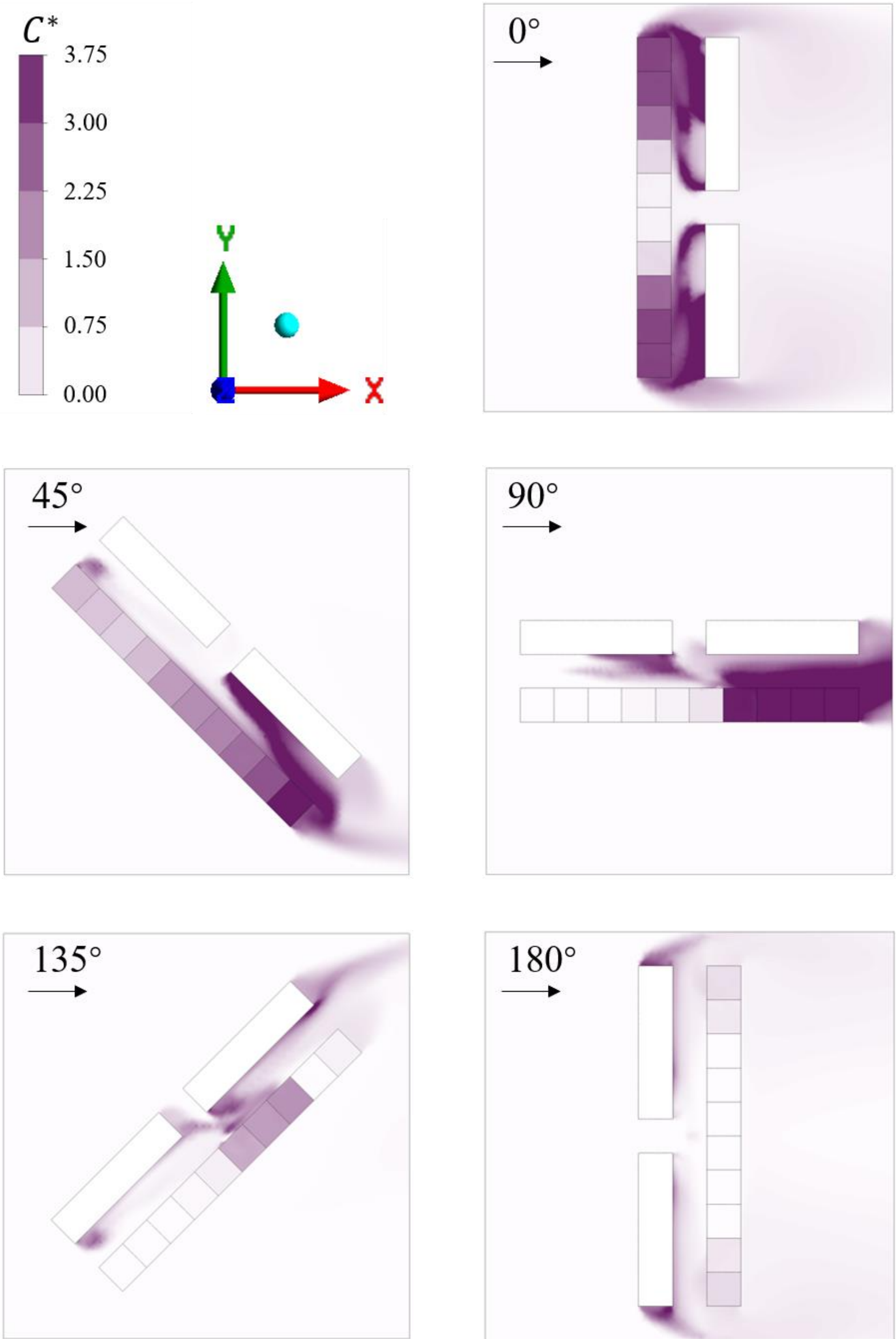

Fig. 14. Case C: C^* at Z = 0.15 m for the five wind directions investigated.

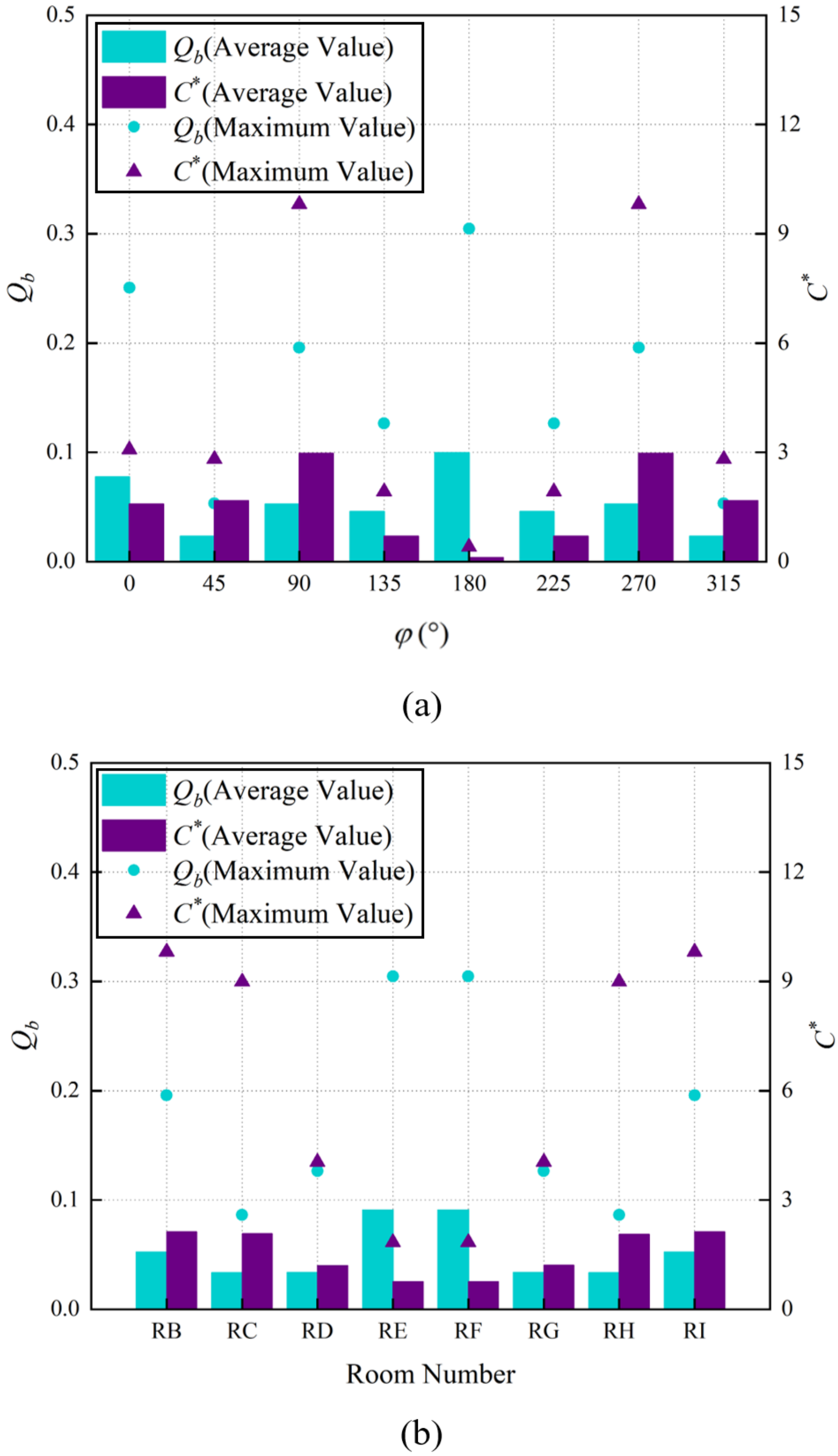

Fig. 15. Comparison of (a) Q_b (b) C^* for all the cases investigated.

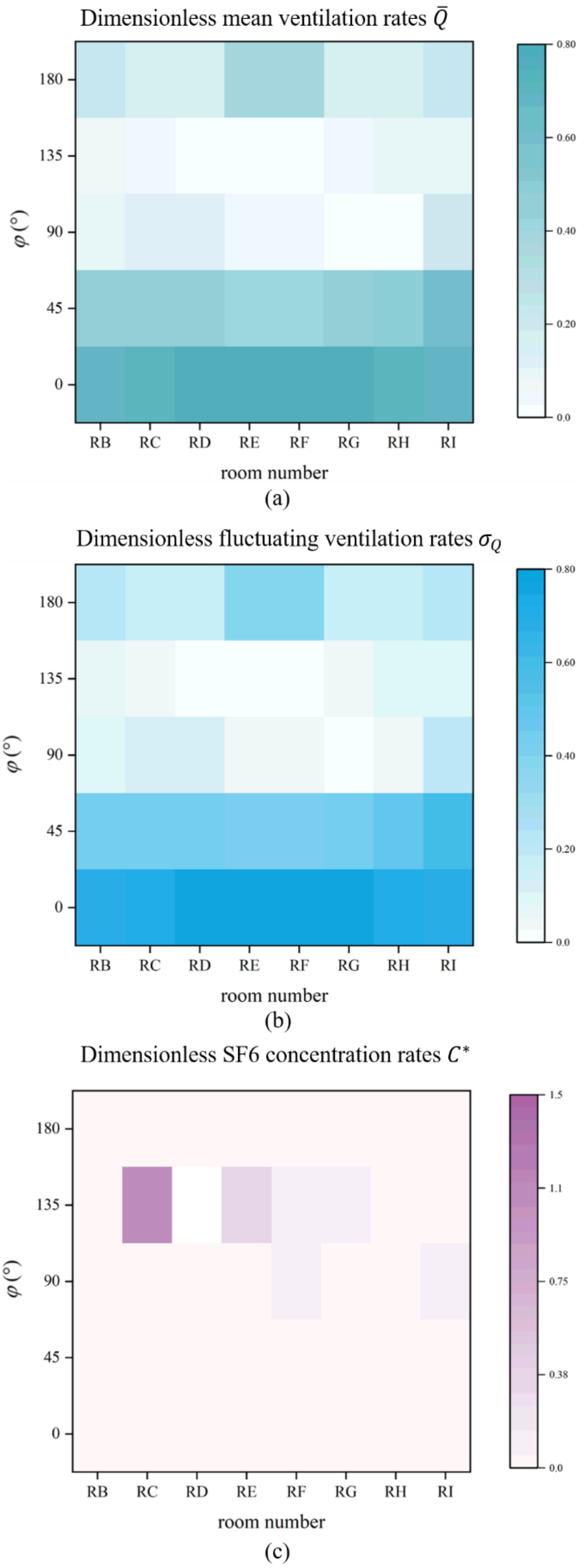

Fig. 16. The dimensionless mean and fluctuating ventilation rates and C^* for Case D under different wind directions.

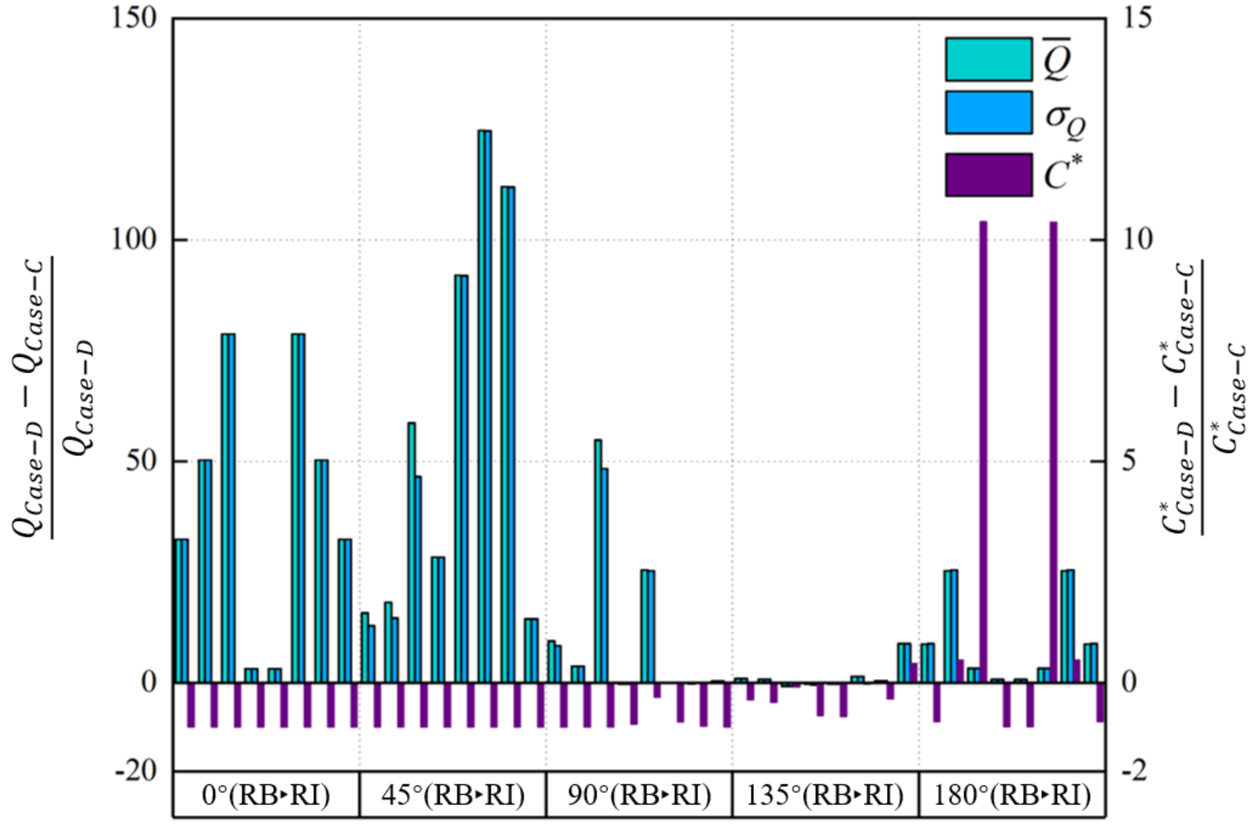

Fig. 17. Variation of the ventilation rate of Case D compared to Case C.

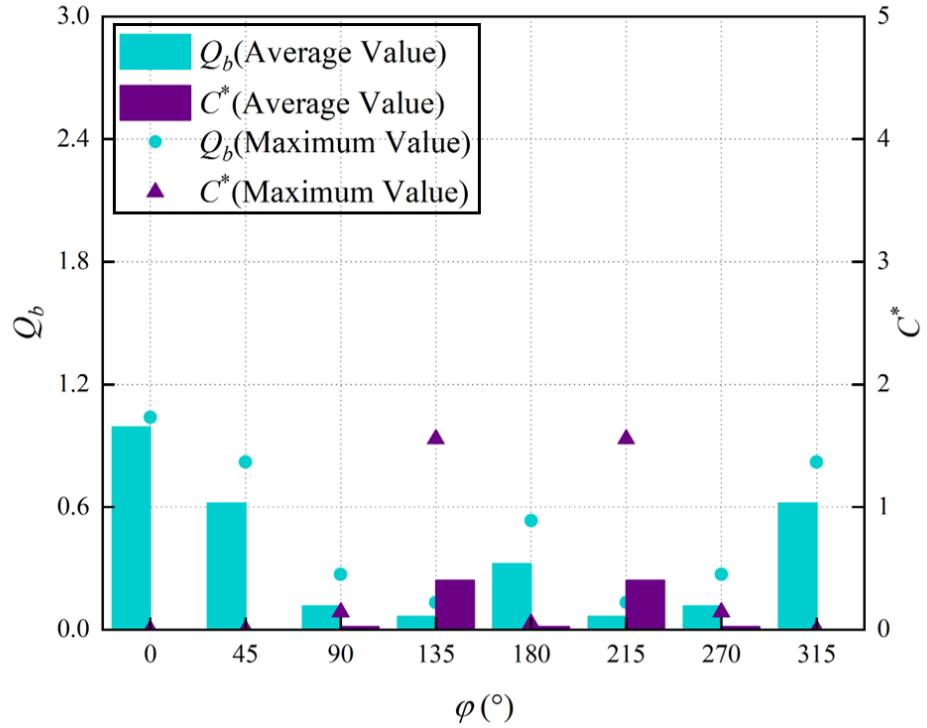

(a)

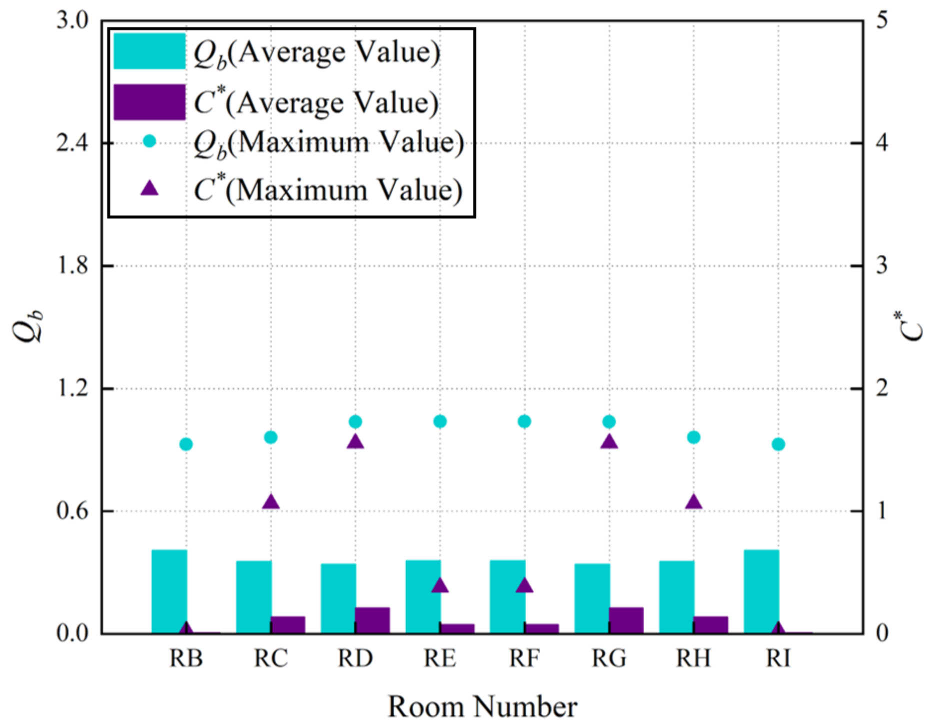

(b)

Fig. 18. Comparison of (a) Q_b (b) C^* for Case D investigated.

Table 1

Solver settings and boundary conditions.

CFD procedure	SRANS	URANS
Turbulent model	SST k-ω	
Pressure-velocity coupling	SIMPLEC	PISO (First-order implicit)
Discretization scheme for advection term	Second-order upwind difference scheme	
Discretization scheme for diffusion term	Second-order central difference scheme	
Calculation duration	2000 iterations	100000 time steps
Time step size	/	Δt = 0.001 s
Sampling length	/	60000 time steps
Residuals	$<10^{-5}$	$<10^{-7}$
Inlet boundary condition	Velocity inlet: $\frac{U(z)}{U_H}=\left(\frac{z}{H}\right)^{\alpha}$, $k(z)=\left(I(z)U(z)\right)^2$ $\omega(z)=\frac{\varepsilon(z)}{k(z)C_\mu}$	
Outlet boundary condition	Outflow (zero normal gradient)	
Other boundary conditions	No-slip wall	

Table 2

Details of coarse, medium and fine grids.

Grid	y^+	Δy	γ	Boundary layer number	Total mesh number
Coarse	5	0.7mm	1.2	8	2.79million
Medium	3	0.17mm	1.15	12	3.56million
Fine	1	0.058mm	1.1	16	6.27million

Table 3

Percentage difference of GCI values among different mesh sizes for lines L1, L2, L3, L4, L5 and L6.

GCI Values		L1	L2	L3	L4	L5	L6
Medium-Fine	*U*	1.06%	1.02%	0.96%	0.11%	0.95%	0.42%
	C	0.64%	0.31%	0.12%	0.49%	0.12%	0.11%
Coarse-Fine	*U*	5.03%	4.46%	5.18%	0.96%	2.21%	1.08%
	C	1.17%	0.82%	2.01%	0.87%	1.03%	0.77%

Table 4

Validation metrics calculated for normalized mean concentration C^* of Wall A and Wall B.

Validation metrics (ideal value)	**Range**	**Membership function**	***C****	
			Line 1 (Wall A)	**Line 2 (Wall B)**
FB, Fractional Bias (**0**)	-0.3 < FB < 0.3	**Good**	**-0.192**	**0.206**
	0.3 < |FB| < 1.33	**Fair**		
	|FB| > 1.33	**Poor**		
NMSE, Normalized Mean Square Error (**0**)	NMSE < 3	**Good**	**0.239**	**0.043**
	9 < NMSE < 16	**Fair**		
	NMSE > 25	**Poor**		
NAD, Normalized Absolute Difference (**0**)	NAD < 0.3	**Good**	**0.096**	**0.103**
	0.3 < NAD < 0.5	**Fair**		
	NAD > 0.5	**Poor**		
FAC2, within a factor of two (**1**)	FAC2 > 0.5	**Good**	**0.606**	**0.615**
	0.3 < FAC2 < 0.4	**Fair**		
	FAC2 < 0.2	**Poor**		